Journal of Marine Science and Technology
https://doi.org/10.1007/s00773-024-01031-1

ORIGINAL ARTICLE

Development of a mathematical model for harbor maneuvers to realize modeling automation

Yoshiki Miyauchi[1] · **Youhei Akimoto**[2,3] · **Atsuo Maki**[1]

Received: 25 February 2023 / Accepted: 23 September 2024

Abstract
A simulation environment of harbor maneuvers is critical for developing automatic berthing. Mathematical models are widely used to estimate harbor maneuvers. However, user's analysis and decision are necessary to derive, select, and identify the model because each actuator configuration needs an inherent mathematical expression. We proposed a new mathematical model for arbitrary configurations to overcome that issue. The new model is a hybrid model that combines the simplicity of the derivation of the Taylor expansion and the high degree of freedom of the MMG low-speed maneuvering model. We also developed a method to select mathematical expressions for the proposed model using system identification. Because the proposed model can easily derive mathematical expressions, we can generate multiple expressions simultaneously and choose the best one. This method can reduce the workload of model identification and selection. Furthermore, the proposed method will enable the automatic generation of mathematical models because it can reduce user's decision-making and data analysis for the model generation due to its less dependency on the knowledge of ship hydrodynamics and captive model test. The proposed method was validated with free-running model tests and showed equivalent or better estimation performance than the conventional model generation method.

Keywords Ship maneuvering · Autonomous docking · Maneuvering model · System identification · CMA-ES

1 Introduction

Research and development of Maritime Autonomous Surface Ship (MASS) are active, including automatic berthing. The development of controllers for MASS—including parameter tuning, verification, and certification by class society—ultimately requires verification in a real ship. Still, a significant part of development in a simulation environment would be helpful from a cost and safety. A mathematical model of a ship's maneuver (i.e., maneuvering model or system-based mathematical model hereafter simply referred to as "mathematical model" or the "model") is widely used to estimate ship maneuvering in numerical simulations from the standpoint of computation time.

The harbor maneuver of a ship is an inclusive maneuver that includes various maneuvers: leaving and entering the port, approach maneuvers to the berth, berthing, and also unberthing; hence, it contains various types of motions, i.e., forward, astern, acceleration and deceleration, turn, pivot turn, stop, crabbing, position-keeping. A mathematical model for harbor maneuvers is generally more complex than that for ocean navigation because the flow field and use of actuators are much more complex and because the ship is navigating close to obstacles, the high estimation accuracy is required.

Mathematical models for harbor maneuvers can be divided into two categories how they address the complexity, either a complex model that switches and combines submodel withvarious condition, or a simpler one that uses unified mathematical expression and parameters for all state for practicality. The former method is represented by the low-speed maneuvering MMG model [e.g., 1, 2], and the latter

✉ Yoshiki Miyauchi
yoshiki_miyauchi@naoe.eng.osaka-u.ac.jp

Atsuo Maki
maki@naoe.eng.osaka-u.ac.jp

[1] Osaka University, 2-1 Yamadaoka, Suita, Osaka, Japan

[2] Faculty of Engineering, Information and Systems, University of Tsukuba, 1-1-1 Tennodai, 305-8573 Tsukuba, Ibaraki, Japan

[3] RIKEN Center for Advanced Intelligence Project, 1-4-1 Nihonbashi, Chuo-ku, 103-0027 Tokyo, Japan

Published online: 17 October 2024

is represented by Abkowitz model with variable propeller rotation [3] and Fossen's model for dynamic positioning [4].

1.1 Problem definition

Generating a maneuvering model of a particular ship generally consists of the following four tasks. Therefore, in this paper, the term "model generation" refers to the entire process that includes the following four tasks, and, a "user" is a person who generates a model and utilizes the model in a simulation environment.

Derivation of the model's mathematical expression The user derives a new mathematical model if the existing model is not sufficient. The derivation here refers to the derivation of the mathematical expressions of the model. This step is unnecessary if the user thinks an existing model is sufficient.

Model selection The user selects the mathematical model to be used. The selection is based on the findings of previous studies or results of maneuvering basin tests conducted by the user.

Parameter identification The user obtains model parameters for the selected model from maneuvering basin tests, databases, or empirical formulae.

Validate mathematical model The user performs a maneuvering simulation with identified model parametersmathematical model. The model is validated by comparing the simulation results with known maneuvers, a maneuvering trial of a ship or a free-running model ship.

1.2 Difficulties of existing modeling methods

Let us assume that the user's goal is to build a maneuvering simulation environment that can simulate harbor maneuvers. If the hull form of the ship is fixed and the accuracy of maneuvering simulation is required, model parameters are often identified by the captive model test [5–7]. The standard method of the MMG model [7] also uses captive model tests to identify model parameters. Moreover, even for harbor maneuvers, several studied [8–15] on berthing control have used captive model tests to identify model parameters. However, existing mathematical models and captive model test-based scheme seem problematic because the user's workload to generate the model is large. In particular, the following are some examples:

Special testing facility The model parameters are obtained from hydrodynamic forces measured in a towing tank or a maneuvering basin; hence, the model cannot be generated without using such a facility. Recently, computational fluid dynamics (CFD) has been used to alternate captive model tests [16–18]. However, powerful computational resources and CFD expertise are required.

Cost of parameter identification The time and the cost required for the experiment become non-negligible due to the increased number of test conditions caused by the complexity of the model of harbor maneuvers.

Selection of the mathematical model. So far, several mathematical models have been proposed that are applicable to harbor maneuvers (see Sect. 1.3), but none of them can be called the de facto standard yet. Therefore, the user must select an appropriate model (and its mathematical expression) for their vessel of interest. Selection can be done by comparing various models with a known maneuver or comparing estimated hydrodynamic forces with captive model tests.

Diversity of actuator configurations A ship's actuator system includes a wide variety of configurations, e.g., a single-propeller and single-rudder ship, a twin-propeller and twin-rudder ship, a ship with multiple azimuth thrusters, and so on. The mathematical expression of the model is unique to each actuator configuration; thus, the user needs to prepare the model and implement a numerical code for each actuator configuration.

Knowledge of Ship hydrodynamics and model test The user must have appropriate knowledge of captive model tests, hydrodynamics on ship maneuvering, and the model itself to identify model parameters from captive model tests. However, for the users who aim to build automatic berthing systems, those knowledge is not necessarily their area of expertise. In such cases, a different person who is an expert in that area should be asked for support.

1.3 Related works

Among the difficulties stated in Sect. 1.2, "special testing facility" and "cost of parameter identification" can be addressed by the system identification (SI) technique. On the SI for ship maneuvering, SI identifies model parameters from a set of ship trajectories. SI for ship maneuvering was first introduced by Äström and Köllström [19], and Abkowitz [3] in the late 1970s and early 1980s, and then numerous studies have been done for both from full-scale[3, 19–21] ship and model ship [22–25].

However, research on SI has been conducted mainly on mathematical models for IMO standard maneuvers [26], ocean voyage, and autopilot application. Only a few studies have been conducted on SI for mathematical models on harbor maneuvers. The authors previously studied [1] the feasibility of SI for low-speed maneuvering MMG model for single-propeller, single rudder ship. The MMG model used in the previous study [1] can represent characteristics of harbor maneuvers, e.g., large drift angle, thrust reduction on propeller reversal, and rudder characteristics dependency on propeller wake. Model parameters were identified from trajectories for the scaled free-running model. SI of low-speed maneuvering MMG model for single-propeller, single rudder ship was also done by Sawada et al. [27]. In [27], they

used full-scale ship trial data as train data and succeeded in developing a berthing controller with a simulation environment using the identified model. Using Fossen's model [4], SI of an urban ferry with azimuth thrusters was done by [28].

All of the above previous research [1, 27, 28] used mathematical models which categorized as the Hydrodynamic model [29]. The hydrodynamic model is a model that was derived and designed to identify the model parameters based on hydrodynamic assumption, observation, and measurement. The other kind of model is the response model [29], which considers only the relationship between the ship's control input and response, i.e., the motion of the ship. The most popular response model would be Nomoto's KT model [30]. Meanwhile, application of neural networks (NN) as a response model has been actively studied in the last two decades [31–33]. Models using NN are highly capable of modeling the nonlinear dynamics; however, to the best of our knowledge, Wakita et al. [34] is the only case of SI using NN for harbor maneuvers.

1.4 Objective and contribution of the study

We recognize that to overcome the remaining difficulties—selection of a model, diversity of actuator configurations, and knowledge of ship hydrodynamics—a new response model-type model is necessary. The hydrodynamic model has a favorable feature that the physical meaning of the formulae is understandable; therefore, flow field and forces can be observed from the model. However, it needs to derive model formulae with due consideration of hydrodynamics for each configuration. On the other hand, as a simulation environment for R &D of automatic berthing, how the ship moves, i.e., the relationship between the control input and response, is important. Whether the mathematical model can represent the flow field and hydrodynamic forces is desirable but not mandatory. Hence, the response model, especially a model using NN, is an option to overcome those issues; however, behavior on the extrapolation region of train data is questionable because the model is not understandable and needs treatment to impose a constraint to be physically reasonable (e.g., [34]).

Therefore, we aim to propose a new response model whose formulae are easily derivable for arbitrary actuator configurations, have enough degree of freedom to express harbor maneuvers, and not having the downside of NN models. In addition, we aim to propose a method to select formulae of the proposed model which does not depend on captive model tests and knowledge of ship hydrodynamics. Our previous work [35] proposed a 4-quadrant Abkowitz model for single-propeller, single-rudder ships. This previous model was based on Taylor expansion, so the polynomials are easily derived. In addition, the previous model has four sets of model parameters to model the change of characteristics caused by propeller reversal and astern conditions. In this study, we expand the previous model [35] for arbitrary actuators and develop a method for model generation using the SI. Utilizing SI, we will be able to be less dependent on captive model tests and ship hydrodynamics in model generation. Furthermore, the proposed method enables the automatic generation of mathematical models because human intervention in model derivation, selection, and identification can be reduced. Our previous literature [36] described the initial results of the investigations done in this paper. This paper presents the results more extensively, with more details, and with several revisions.

The major contributions of this study are as follows:

1. We proposed a new mathematical model, from which the model formula is easily derived according to simple rules and is complex enough to handle complex phenomena of harbor maneuvers. The new model is a hybrid model that combines the simplicity of the derivation of the Abkowitz model, based on Taylor expansion, and the complexity of the MMG low-speed maneuvering model.
2. We proposed a method for selecting a model that does not require captive model tests and knowledge of ship hydrodynamics and modeling. Because the proposed model can easily derive multiple formulae, we can generate multiple models using system identification and select the model formulae that best fit the ship's trajectory. Therefore, we can reduce the effort of parameter identification and model selection for arbitrary actuator configurations.

2 Abkowitz–MMG hybrid model

2.1 Overview of the proposed model

This section describes the mathematical model proposed in this study (hereafter referred to as the "proposed model"). The proposed model is a hybrid model that combines the simplicity of the Abkowitz model with the complexity of the MMG low-speed model.

Requirements of the model First, we describe the requirements of the proposed model and ideas of our approach to those requirements. The requirements of the proposed model were derived based on the issues raised in the introduction. The requirements are as follows:

Requirement 1 The model complexity can be increased easily. This allows for handling various levels of complexity of the of harbor maneuvers.

Requirement 2 The user can easily derive the model's expression even if the configuration of the actuator of the subject ship changes.

Requirement 3 The model must be accurate enough to evaluate the controller by maneuvering simulation, i.e., the same level of accuracy as existing methods.

Requirement 4 The model can represent significant characteristic changes of fluid forces at berthing and unberthing (e.g., flow separation, propeller reversal).

Requirement 5 Model selection and parameter identification of the proposed model do not require in-depth knowledge of mathematical models or detailed hydrodynamic observation.

Requirement 6 The model does not require captive model tests through its generation process.

Requirement 7 The model has robustness to input state and control input over the operation range of harbor maneuvers. In other words, the divergence of acceleration should not occur even for unknown data within the range of typical harbor maneuvers.

Basic ideas on the model design We designed the proposed model to meet the above requirements with the following ideas:

Idea 1 Following Abkowitz's polynomial model [37] (hereafter, Abkowitz model), the model is derived by Taylor expansion of the hydrodynamic forces. The complexity of the model can be easily increased by increasing the highest degree of the polynomial obtained by Taylor expansion or the number of terms employed (Requirement 1). If the actuator configuration changes (Requirement 2), we only need to add the actuator features (e.g., propeller revolution, rudder angle, azimuth thruster angle) to the Taylor expansion variables.

Idea 2 Following the concept of low-speed maneuvering MMG model, the model parameters are set to different values for each representative condition (e.g., propeller forward/reverse rotation). In addition, the same mathematical expression is maintained for all operating conditions, thereby preserving the simplicity (Requirements 5, 1, 2) while ensuring that the accuracy (Requirement 3) and the complexity (Requirement 4) could be achieved.

Idea 3 Utilize the system identification (SI) and use ship's trajectory (i.e., the time history of motion and actuator usage) as a training dataset to identify the model parameters. Suppose the user can easily derive several different mathematical expressions of the proposed model (Requirement 1), the user can select a model by choosing the one that best fits the motion data for validation. This procedure allows the user to select the appropriate model without requiring observation of the hydrodynamic forces or knowledge of the model (Requirement 5). It also achieves a captive model test-free.

Idea 4 The stability of the proposed model is not ensured because the model's expressions and parameter exploration domain are not based on hydrodynamics. Therefore, we intended to maintain the stability of the proposed model by the objective function and the dataset to be used in the optimization process. Details of the objective function and dataset are described in Sects. 3.1 and 3.3, respectively.

2.2 Derivation of proposed model

In this section, we derive the mathematical expression of the proposed model based on the basic idea described in the previous section. First, the subject ship is a scaled model ship of a coastal vessel equipped with a single-propeller, VecTwin type twin-rudder, and bow thruster. The ship fixed coordinate system $\mathrm{O}-xy$ and space fixed coordinate system $\mathrm{O}_0-x_0y_0$ are defined as Fig. 1 and equations of motion for the three degrees of freedom used in the standard MMG model [7] are as follows:

$$\begin{aligned}
&(m+m_x)\dot{u}-(m+m_y)v_m r-x_G m r^2=X\\
&(m+m_y)\dot{v}_m+(m+m_x)ur+x_G m\dot{r}=Y\\
&(I_{zz}+J_{zz}+x_G^2 m)\dot{r}+x_G m(\dot{v}_m+ur)=N.
\end{aligned} \tag{1}$$

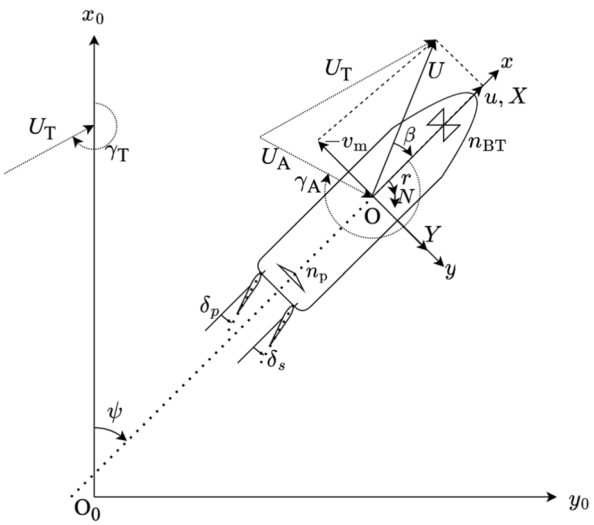

Fig. 1 Coordinate systems

Here, notations for physical parameters are as follows: m is ship's mass, I_{zz} is the moment of inertia at the center of gravity (CG), m_x and m_y are added mass, J_{zz} is added inertia moment, x_G is the longitudinal distance to CG from midship, $X,\ Y,\ N$ are forces and moment acting on the body except added mass. Notations for kinematic variables are as follows: ψ is ship heading, u and v_m are longitudinal and lateral speed of motion on $O-xy$ system, r is yaw angular velocity, β is drift angle, and $(\dot{\cdot})$ represent the time derivative. Notations for actuator features are as follows: n_P and n_BT are revolution numbers of propeller and bow thruster, $\delta_\mathrm{s},\ \delta_\mathrm{p}$ are rudder angles of starboard and port side rudder. Notations for wind are as follows: U_T and γ_T are true wind speed and direction, U_A and γ_A are apparent wind speed and direction, respectively.

Next, the right-hand side of Eq. 1 is expressed as a polynomial by Taylor expansion. The classical Abkowitz model assumes the perturbation motion of a ship from a certain forward speed $u = U_0,\ v = 0,\ r = 0$. Then, expand the hydrodynamic forces or their dimensionless forms by the state variables $\boldsymbol{s}_t$, the control vectors $\boldsymbol{a}_t$ and their time derivatives $\dot{\boldsymbol{s}}_t,\ \dot{\boldsymbol{a}}_t$. To apply Abkowitz model to harbor maneuvers, we use Taylor expansion with ideas below:

Idea 5 Assume that hydrodynamic forces and moments are function of $\boldsymbol{s}_t$, $\boldsymbol{a}_t$ and added mass component on left hand side of Eq. 1. The users can include other added mass components and $\dot{\boldsymbol{a}}_t$ in the model if necessary, however generally those are neglected in MMG model.

Idea 6 No scale conversion is performed since we assumed that the user estimates the model directly from the motion of a full-scale ship. This means that the hydrodynamic forces are expanded by Taylor expansion without non-dimensionalization. This is also because to avoid zero division caused by the non-dimensionalization[1] of the hydrodynamic forces at $U = 0$.

Idea 7 Assuming slow-speed motion, hydrodynamic forces are expanded around the origin ($\boldsymbol{s}_t = 0,\ \boldsymbol{a}_t = 0$) by Taylor's expansion.

Idea 8 Hydrodynamic forces are decomposed into the above-water (wind) and below-water (underwater) contributions to account for the wind force, which is relatively important in harbor maneuvers. This decomposition is appropriate because the relative wind velocity governs the wind force while ship's state and control input governs the underwater contribution. While the underwater contribution is Taylor expanded, the wind force is modeled using an existing wind force model.

Accordingly, let us start the derivation of the mathematical model from the decomposition of the hydrodynamic forces on the right-hand side of the Idea 8 into wind pressure forces $X_\mathrm{A},\ Y_\mathrm{A},\ N_\mathrm{A}$ and other hydrodynamic forces. Next, let us focus on hydrodynamic forces acting below the water surface. Since the subject ship has a bow thruster, the following is assumed.

- Bow thruster force Y_BT, N_BT is separated with the hydrodynamic forces of the hull+rudder+propeller X_HPR, Y_HPR, N_HPR, because bow thruster is located at the bow, away from the rudder and propeller, so we assume that the influence of the flow interaction between bow thruster and rudder/propeller is small. If this were a stern thruster, the coupling with the propeller and rudder would need to be considered.
- Bow thruster is assumed that it does not generate force in the X direction.

From these assumptions, we yield the following:

$$X = X_\mathrm{HPR} + X_\mathrm{A} \tag{2}$$

$$Y = Y_\mathrm{HPR} + Y_\mathrm{BT} + Y_\mathrm{A} \tag{3}$$

$$N = N_\mathrm{HPR} + N_\mathrm{BT} + N_\mathrm{A}. \tag{4}$$

The wind force $X_\mathrm{A},\ Y_\mathrm{A},\ N_\mathrm{A}$ is modeled by existing polynomial-type model (see Sect. 2.3) proposed by [38]. The coefficients of the wind force model were optimized simultaneously with the coefficients of $X_\mathrm{HPR},\ Y_\mathrm{HPR},\ N_\mathrm{HPR}$ by SI. As a first step of research, bow thruster was neglected, although the subject ship is equipped with a bow thruster; therefore, always $Y_\mathrm{BT} = N_\mathrm{BT} = 0$.

Next, we select the variable vector $\boldsymbol{x} = (\boldsymbol{s}_t,\ \boldsymbol{a}_t)$ for Taylor expansion of $X_\mathrm{HPR},\ Y_\mathrm{HPR},\ N_\mathrm{HPR}$. We selected following variables for state variables vector $\boldsymbol{s}_t$ and control input vector $\boldsymbol{a}_t$, where the subscript t is the value at time t:

$$\boldsymbol{s}_t \equiv (u,\ v_\mathrm{m},\ r) \in \mathbb{R}^3 \tag{5}$$

$$\boldsymbol{a}_t \equiv (n_\mathrm{P},\ \sin(\delta_\mathrm{s}),\ \cos(\delta_\mathrm{s}),\ \sin(\delta_\mathrm{p}),\ \cos(\delta_\mathrm{p})) \in \mathbb{R}^5. \tag{6}$$

Here, we use trigonometric functions of the rudder angles $\delta_\mathrm{s},\ \delta_\mathrm{p}$ for the port and starboard rudder features. Most Abkowitz models use the rudder angle δ, but trigonometric functions of the rudder angles are physically appropriate to express rudder forces to decompose the rudder normal force with a trigonometric function, as in the MMG model [7, 29]. In addition, the proposed model is intended to be able

[1] $X' = X/(0.5\rho LdU^2),\ Y' = Y/(0.5\rho LdU^2),\ N' = N/(0.5\rho L^2)dU^2)$

to apply arbitrary actuator configurations. Model formulae need to be capable of representing the post-stall characteristics of the rudder to represent high-lift rudder systems such as the Vectwin rudder system we employed in this study. The Vectwin rudder can steer up to 105°, which is in the post-stall region. The use of a trigonometric function of the rudder angle instead of the rudder angle itself allows for more degrees of freedom in model formulae without increasing the number of variables to be optimized. At the same time, the use of radian may induce overestimation of rudder force where the rudder effectiveness is in the post-stall region.

If the user wants to derive the mathematical model for other ship configurations, add appropriate features to $\boldsymbol{a}_t$. For example, for a ship equipped with a stern thruster, the revolution number of the stern thruster can be added to $\boldsymbol{a}_t$. Likewise, the revolution number of the azimuth thruster and the sin and cos functions of the operating angle can be used for an azimuth thruster.In addition, if the user needs to consider the shallow water effect in the harbor, we can add under keel clearance h to the variable vector $\boldsymbol{x}$.

2.2.1 Derivation of mathematical expressions by Taylor expansion

Taylor expansion is now performed for X_{HPR}, Y_{HPR}, and N_{HPR}. Hereafter we only show the manipulation for X_{HPR}, but Y_{HPR} and N_{HPR} are also derived similarly. X_{HPR} is expanded for $\boldsymbol{x}$ as follows:

$$\begin{aligned} &X_{\mathrm{HPR}}(x_1,\ \ldots,\ x_k) \\ &\quad = X_{\mathrm{HPR}}(x_1,\ \ldots,\ x_k)\big|_{\boldsymbol{x}=0} \\ &\qquad + \frac{1}{1!}\left(\sum_{i=1}^{k} x_i \frac{\partial}{\partial x_i}\bigg|_{\boldsymbol{x}=0}\right) X_{\mathrm{HPR}}(x_1,\ \ldots,\ x_k) \\ &\qquad + \frac{1}{2!}\left(\sum_{i=1}^{k} x_i \frac{\partial}{\partial x_i}\bigg|_{\boldsymbol{x}=0}\right)^2 X_{\mathrm{HPR}}(x_1,\ \ldots,\ x_k) \\ &\qquad + \frac{1}{3!}\left(\sum_{i=1}^{k} x_i \frac{\partial}{\partial x_i}\bigg|_{\boldsymbol{x}=0}\right)^3 X_{\mathrm{HPR}}(x_1,\ \ldots,\ x_k) \\ &\qquad + \cdots, \end{aligned} \tag{7}$$

where

$$\begin{aligned} \boldsymbol{x} &= (x_1,\ \ldots,\ x_k) \\ &= \left(u,\ v_{\mathrm{m}},\ r,\ n_{\mathrm{P}},\ \sin(\delta_{\mathrm{s}}),\ \cos(\delta_{\mathrm{s}}),\ \sin(\delta_{\mathrm{p}}),\ \cos(\delta_{\mathrm{p}})\right) \in \mathbb{R}^8. \end{aligned} \tag{8}$$

Ignoring the fluid memory effect, we can assume that $X_{\mathrm{HPR}}(x_1,\ \ldots,\ x_k)\big|_{\boldsymbol{x}=0} = 0$. Then the first term on the right-hand side of the Eq. 7 can be ignored. Next, expanding Eq. 7, we obtain

$$\begin{aligned} &X_{\mathrm{HPR}}(\boldsymbol{s}_t, \boldsymbol{a}_t) \\ &\quad = \frac{\partial X_{\mathrm{HPR}}}{\partial u}\bigg|_{\boldsymbol{x}=0} u + \frac{\partial X_{\mathrm{HPR}}}{\partial v_{\mathrm{m}}}\bigg|_{\boldsymbol{x}=0} v_{\mathrm{m}} + \cdots \\ &\qquad + \frac{1}{2!}\left(\frac{\partial^2 X_{\mathrm{HPR}}}{\partial u^2}\bigg|_{\boldsymbol{x}=0} u^2 + \ldots \frac{\partial^2 X_{\mathrm{HPR}}}{\partial \cos^2\delta_{\mathrm{p}}}\bigg|_{\boldsymbol{x}=0} \cos^2\delta_{\mathrm{p}}\right) \\ &\qquad + \frac{1}{3!}\left(\frac{\partial^3 X_{\mathrm{HPR}}}{\partial u^3}\bigg|_{\boldsymbol{x}=0} u^3 + \cdots + \frac{\partial^3 X_{\mathrm{HPR}}}{\partial \cos^3\delta_{\mathrm{p}}}\bigg|_{\boldsymbol{x}=0} \cos^3\delta_{\mathrm{p}}\right) + \cdots. \end{aligned} \tag{9}$$

Partial derivatives of Eq. 9 are called hydrodynamic coefficients on Abkowitz model. Using common expressions of hydrodynamic coefficients, we can formulate Eq. 9 as follows,

$$\begin{aligned} &X_{\mathrm{HPR}}(\boldsymbol{s}_t, \boldsymbol{a}_t) \\ &\quad = X_u u + \ldots + X_{\cos(\delta_{\mathrm{p}})}\cos(\delta_{\mathrm{p}}) \\ &\quad + X_{uu}u^2 + \ldots + X_{\cos(\delta_{\mathrm{p}})\cos(\delta_{\mathrm{p}})}\cos^2(\delta_{\mathrm{p}}) \\ &\quad + X_{uuu}u^3 + \ldots + X_{\cos(\delta_{\mathrm{p}})\cos(\delta_{\mathrm{p}})\cos(\delta_{\mathrm{p}})}\cos^3(\delta_{\mathrm{p}}) \\ &\quad + \cdots, \end{aligned} \tag{10}$$

where

$$\begin{aligned} X_{x_i} &\equiv \frac{\partial X_{\mathrm{HPR}}}{\partial x_i}\bigg|_{\boldsymbol{x}=0} \\ X_{x_i x_j} &\equiv \frac{1}{2!}\frac{\partial^2 X_{\mathrm{HPR}}}{\partial x_i \partial x_j}\bigg|_{\boldsymbol{x}=0} \\ X_{x_i x_j x_k} &\equiv \frac{1}{3!}\frac{\partial^3 X_{\mathrm{HPR}}}{\partial x_i \partial x_j \partial x_k}\bigg|_{\boldsymbol{x}=0}. \end{aligned} \tag{11}$$

2.2.2 Selection of the term of polynomial equation

For polynomial-type mathematical models, the question is which terms in Eq. 10 should be included in the polynomial. For existing mathematical models, the choice of formulae has been determined by comparison with the results of captive model tests. For example, for of MMG, see [39, 40], and for Abkowitz model see [6]. However, in this study, we assume a captive model test-free mathematical model (Requirement 6). Therefore, the proposed model's order and term selection methods are as follows:

Idea 9 All terms are used unless they are obviously unnecessary or need modification.

Idea 10 The highest order of the polynomials is defined by the capability of the optimization method and the user's computational resources. The user derives and compares several model formulae with different maximum order. In this study, second- and third-order models were used.

The reasons are as follows: the available duration of the test facility for the captive model test-based method binds the number of identifiable parameters. For example, the original Abkowitz model [37] used 65 parameters, and studies by the authors using the MMG low-speed maneuvering model [1] used 52 parameters to model the forces acting below the surface of the water. The authors believe that about 100 is a practical upper limit for the number of model parameters. To ensure accuracy with fewer terms, the terms employed should be examined based on theoretical considerations and observations on the hydrodynamics forces. On the other hand, SI can increase the number of parameters as far as the performance of the optimization method allows. For example, CMA-ES used in this study (described in detail in Sect. 3.5) can optimize up to several hundred dimensions. The proposed model is assumed to be a model that does not require detailed observation of the hydrodynamic forces; thus, terms are removed or modified only for obvious ones.

Based on the principles discussed above, we perform modification of Eq. 10. The proposed model is modified with the following three manipulations.

Modification A: selection based on the symmetricity of the ship The term is selected based on the fact that the ship is symmetrical at the longitudinal center line of the hull. Original Abkowitz model [37] assumed for a single-propeller, single-rudder ship; hence, X is assumed as an even function of v_m,[2] r, δ. Hence, the odd powers of v_m, r, δ were deleted from the polynomial for X. Similarly, because Y and N were assumed as an odd function of v_m, r, δ due to symmetry, their even powers were deleted.

The proposed model also uses this symmetry assumption. We assume that X is an even function of $\boldsymbol{x}_\mathrm{asym} = \{v_\mathrm{m},\ r,\ \sin(\delta_\mathrm{s}),\ \sin(\delta_\mathrm{p})\}$, and remove the odd power terms $\sum_{i=1,3,\ldots}\{v_\mathrm{m} + r + \sin(\delta_\mathrm{s}) + \sin(\delta_\mathrm{p})\}^i$. Also, from the polynomial of Y and N, the 0th power and even power terms $\sum_{i=0,2,\ldots}\{v_\mathrm{m} + r + \sin(\delta_\mathrm{s}) + \sin(\delta_\mathrm{p})\}^i$ were removed. The asymmetric motion vector $\boldsymbol{x}_\mathrm{asym}$ was selected for motions outside the symmetry plane of the hull.

However, strictly speaking, Y and N are asymmetric and hence not purely odd functions of $\boldsymbol{x}_\mathrm{asym}$. For example, for a single-propeller ship, turning forces of the port and starboard sides are different due to the rotational flow of the propeller. In addition, significant lateral force and yaw moment will occur during propeller reversal of a single-fixed-pitch propeller ship [41–43]. That asymmetricity can be modeled by not removing the 0th powered term of $\boldsymbol{x}_\mathrm{asym}$ (e.g., Y_u, Y_{uu}, …) [37]. However, we decided not to add terms to express asymmetricity to prioritize the simplicity of the model derivation.

Modification B: delete terms containing nth power of $\sin(\cdot)$ and $\cos(\cdot)$ Terms containing the n-th power of the trigonometric function of the rudder angle were removed, except for $n = 1$. Further consideration of the physical meaning of the power function of the rudder angle is necessary. However, here we removed those to maintain the optimization dimension reasonably.

Modification C: replace squared variables with modulus function Replace the squared variable, both on the 2nd-order term and 3rd-order term, with the modulus function. For the X polynomial, replace x_k^2 for $x_k \notin \boldsymbol{x}_\mathrm{asym}$ to $x_k|x_k|$ and similarly in the Y, N polynomial, $x_k \in \boldsymbol{x}_\mathrm{asym}$, let x_k^2 be $x_k|x_k|$. However, this is not done for odd power terms of non-coupling terms, such as uuu and $v_\mathrm{m}v_\mathrm{m}v_\mathrm{m}$.

The results of the above operations are shown below. Here let us express the obtained polynomial for 3rd-order model as the inner product of hydrodynamic coefficient vector $\boldsymbol{X}^{(i)} \in \mathbb{R}^m$, $\boldsymbol{Y}^{(i)} \in \mathbb{R}^n$, or $\boldsymbol{N}^{(i)} \in \mathbb{R}^n$ and even powers vector $\boldsymbol{z}_\mathrm{even} \in \mathbb{R}^m$ of $\boldsymbol{x}_\mathrm{asym}$ or odd powers vector $\boldsymbol{z}_\mathrm{odd} \in \mathbb{R}^n$, as follows:

$$
\begin{aligned}
X_\mathrm{HPR} &= \boldsymbol{X}^{(i)} \cdot \boldsymbol{z}_\mathrm{even} \\
Y_\mathrm{HPR} &= \boldsymbol{Y}^{(i)} \cdot \boldsymbol{z}_\mathrm{odd} \\
N_\mathrm{HPR} &= \boldsymbol{N}^{(i)} \cdot \boldsymbol{z}_\mathrm{odd},
\end{aligned}
\tag{12}
$$

where

$$
\begin{aligned}
\boldsymbol{X}^{(i=1\cdots m)} = \big(&X_u^{(i)},\ X_{\cos(\delta_\mathrm{s})}^{(i)},\ X_{\cos(\delta_\mathrm{p})}^{(i)},\ X_{n_\mathrm{P}}^{(i)}, \\
&X_{u|u|}^{(i)},\ X_{u\cos(\delta_\mathrm{s})}^{(i)},\ X_{u\cos(\delta_\mathrm{p})}^{(i)},\ X_{un_\mathrm{P}}^{(i)},\ X_{v_\mathrm{m}v_\mathrm{m}}^{(i)}, \\
&X_{v_\mathrm{m}r}^{(i)},\ X_{v_\mathrm{m}\sin(\delta_\mathrm{s})}^{(i)},\ X_{v_\mathrm{m}\sin(\delta_\mathrm{p})}^{(i)},\ X_{rr}^{(i)},\ X_{r\sin(\delta_\mathrm{s})}^{(i)}, \\
&X_{r\sin(\delta_\mathrm{p})}^{(i)},\ X_{\sin(\delta_\mathrm{s})\sin(\delta_\mathrm{p})}^{(i)},\ X_{\cos(\delta_\mathrm{s})\cos(\delta_\mathrm{p})}^{(i)}, \\
&X_{\cos(\delta_\mathrm{s})n_\mathrm{P}}^{(i)},\ X_{\cos(\delta_\mathrm{p})n_\mathrm{P}}^{(i)},\ X_{n_\mathrm{P}|n_\mathrm{P}|}^{(i)}, \\
&X_{uuu}^{(i)},\ X_{uv_\mathrm{m}v_\mathrm{m}}^{(i)},\ X_{uv_\mathrm{m}r}^{(i)},\ X_{urr}^{(i)},\ X_{uv_\mathrm{m}\sin(\delta_\mathrm{s})}^{(i)}, \\
&X_{ur\sin(\delta_\mathrm{s})}^{(i)},\ X_{u|u|\cos(\delta_\mathrm{s})}^{(i)},\ X_{v_\mathrm{m}v_\mathrm{m}\cos(\delta_\mathrm{s})}^{(i)}, \\
&X_{v_\mathrm{m}r\cos(\delta_\mathrm{s})}^{(i)},\ X_{v_\mathrm{m}\sin(\delta_\mathrm{s})\cos(\delta_\mathrm{s})}^{(i)},\ X_{rr\cos(\delta_\mathrm{s})}^{(i)}, \\
&X_{uv_\mathrm{m}\sin(\delta_\mathrm{p})}^{(i)},\ X_{ur\sin(\delta_\mathrm{p})}^{(i)},\ X_{u\sin(\delta_\mathrm{s})\sin(\delta_\mathrm{p})}^{(i)}, \\
&X_{v_\mathrm{m}\cos(\delta_\mathrm{s})\sin(\delta_\mathrm{p})}^{(i)},\ X_{r\cos(\delta_\mathrm{s})\sin(\delta_\mathrm{p})}^{(i)},\ X_{r\sin(\delta_\mathrm{s})\cos(\delta_\mathrm{s})}^{(i)}, \\
&X_{\sin(\delta_\mathrm{s})\cos(\delta_\mathrm{s})\sin(\delta_\mathrm{p})}^{(i)},\ X_{u|u|\cos(\delta_\mathrm{p})}^{(i)},\ X_{u\cos(\delta_\mathrm{s})\cos(\delta_\mathrm{p})}^{(i)}, \\
&X_{v_\mathrm{m}v_\mathrm{m}\cos(\delta_\mathrm{p})}^{(i)},\ X_{v_\mathrm{m}r\cos(\delta_\mathrm{p})}^{(i)}, \\
&X_{v_\mathrm{m}\sin(\delta_\mathrm{s})\cos(\delta_\mathrm{p})}^{(i)},\ X_{v_\mathrm{m}\sin(\delta_\mathrm{p})\cos(\delta_\mathrm{p})}^{(i)},\ X_{rr\cos(\delta_\mathrm{p})}^{(i)}, \\
&X_{r\sin(\delta_\mathrm{s})\cos(\delta_\mathrm{p})}^{(i)},\ X_{r\sin(\delta_\mathrm{p})\cos(\delta_\mathrm{p})}^{(i)},\ X_{\sin(\delta_\mathrm{s})\sin(\delta_\mathrm{p})\cos(\delta_\mathrm{p})}^{(i)}, \\
&X_{u|u|n_\mathrm{P}}^{(i)},\ X_{u\cos(\delta_\mathrm{s})n_\mathrm{P}}^{(i)},\ X_{u\cos(\delta_\mathrm{p})n_\mathrm{P}}^{(i)}, \\
&X_{un_\mathrm{P}|n_\mathrm{P}|}^{(i)},\ X_{v_\mathrm{m}v_\mathrm{m}n_\mathrm{P}}^{(i)},\ X_{v_\mathrm{m}rn_\mathrm{P}}^{(i)}, \\
&X_{v_\mathrm{m}\sin(\delta_\mathrm{s})n_\mathrm{P}}^{(i)},\ X_{v_\mathrm{m}\sin(\delta_\mathrm{p})n_\mathrm{P}}^{(i)},\ X_{rrn_\mathrm{P}}^{(i)},\ X_{r\sin(\delta_\mathrm{s})n_\mathrm{P}}^{(i)}, \\
&X_{r\sin(\delta_\mathrm{p})n_\mathrm{P}}^{(i)},\ X_{\sin(\delta_\mathrm{s})\sin(\delta_\mathrm{p})n_\mathrm{P}}^{(i)},\ X_{\cos(\delta_\mathrm{s})\cos(\delta_\mathrm{p})n_\mathrm{P}}^{(i)}, \\
&X_{\cos(\delta_\mathrm{s})n_\mathrm{P}|n_\mathrm{P}|}^{(i)},\ X_{\cos(\delta_\mathrm{p})n_\mathrm{P}|n_\mathrm{P}|}^{(i)},\ X_{n_\mathrm{P}n_\mathrm{P}n_\mathrm{P}}^{(i)}\big)
\end{aligned}
\tag{13}
$$

[2] Precisely, [37] use the speed at the center of gravity, v_G

$$
\begin{aligned}
z_{\text{even}} = \big(&u,\ \cos(\delta_{\text{s}}),\ \cos(\delta_{\text{p}}),\ n_{\text{P}},\ u|u|,\ u\cos(\delta_{\text{s}}),\\
&u\cos(\delta_{\text{p}}),\ un_{\text{P}},\ v_{\text{m}}v_{\text{m}},\ v_{\text{m}}r,\ v_{\text{m}}\sin(\delta_{\text{s}}),\\
&v_{\text{m}}\sin(\delta_{\text{p}}),\ rr,\ r\sin(\delta_{\text{s}}),\ r\sin(\delta_{\text{p}}),\\
&\sin(\delta_{\text{s}})\sin(\delta_{\text{p}}),\ \cos(\delta_{\text{s}})\cos(\delta_{\text{p}}),\ \cos(\delta_{\text{s}})n_{\text{P}},\\
&\cos(\delta_{\text{p}})n_{\text{P}},\ n_{\text{P}}|n_{\text{P}}|,\\
&uuu,\ uv_{\text{m}}v_{\text{m}},\ uv_{\text{m}}r,\ urr,\ uv_{\text{m}}\sin(\delta_{\text{s}}),\ ur\sin(\delta_{\text{s}}),\\
&u|u|\cos(\delta_{\text{s}}),\ v_{\text{m}}v_{\text{m}}\cos(\delta_{\text{s}}),\ v_{\text{m}}r\cos(\delta_{\text{s}}),\\
&v_{\text{m}}\sin(\delta_{\text{s}})\cos(\delta_{\text{s}}),\ rr\cos(\delta_{\text{s}}),\ r\sin(\delta_{\text{s}})\cos(\delta_{\text{s}}),\\
&uv_{\text{m}}\sin(\delta_{\text{p}}),\ ur\sin(\delta_{\text{p}}),\ u\sin(\delta_{\text{s}})\sin(\delta_{\text{p}}),\\
&v_{\text{m}}\cos(\delta_{\text{s}})\sin(\delta_{\text{p}}),\ r\cos(\delta_{\text{s}})\sin(\delta_{\text{p}}),\\
&\sin(\delta_{\text{s}})\cos(\delta_{\text{s}})\sin(\delta_{\text{p}}),\ u|u|\cos(\delta_{\text{p}}),\\
&u\cos(\delta_{\text{s}})\cos(\delta_{\text{p}}),\ v_{\text{m}}v_{\text{m}}\cos(\delta_{\text{p}}),\ v_{\text{m}}r\cos(\delta_{\text{p}}),\\
&v_{\text{m}}\sin(\delta_{\text{s}})\cos(\delta_{\text{p}}),\ v_{\text{m}}\sin(\delta_{\text{p}})\cos(\delta_{\text{p}}),\ rr\cos(\delta_{\text{p}}),\\
&r\sin(\delta_{\text{s}})\cos(\delta_{\text{p}}),\ r\sin(\delta_{\text{p}})\cos(\delta_{\text{p}}),\\
&\sin(\delta_{\text{s}})\sin(\delta_{\text{p}})\cos(\delta_{\text{p}}),\ u|u|n_{\text{P}},\ u\cos(\delta_{\text{s}})n_{\text{P}},\\
&u\cos(\delta_{\text{p}})n_{\text{P}},\ un_{\text{P}}|n_{\text{P}}|,\ v_{\text{m}}v_{\text{m}}n_{\text{P}},\ v_{\text{m}}rn_{\text{P}},\\
&v_{\text{m}}\sin(\delta_{\text{s}})n_{\text{P}},\ v_{\text{m}}\sin(\delta_{\text{p}})n_{\text{P}},\ rrn_{\text{P}},\ r\sin(\delta_{\text{s}})n_{\text{P}},\\
&r\sin(\delta_{\text{p}})n_{\text{P}},\ \sin(\delta_{\text{s}})\sin(\delta_{\text{p}})n_{\text{P}},\ \cos(\delta_{\text{s}})\cos(\delta_{\text{p}})n_{\text{P}},\\
&\cos(\delta_{\text{s}})n_{\text{P}}|n_{\text{P}}|,\ \cos(\delta_{\text{p}})n_{\text{P}}|n_{\text{P}}|,\ n_{\text{P}}n_{\text{P}}n_{\text{P}}\big)
\end{aligned}
\tag{14}
$$

$$
\begin{aligned}
\boldsymbol{Y}^{(i=1\cdots m)} = \big(&Y^{(i)}_{v_{\text{m}}},\ Y^{(i)}_{r},\ Y^{(i)}_{\sin(\delta_{\text{s}})},\ Y^{(i)}_{\sin(\delta_{\text{p}})},\ Y^{(i)}_{uv_{\text{m}}},\\
&Y^{(i)}_{ur},\ Y^{(i)}_{u\sin(\delta_{\text{s}})},\ Y^{(i)}_{u\sin(\delta_{\text{p}})},\ Y^{(i)}_{v_{\text{m}}\cos(\delta_{\text{s}})},\ Y^{(i)}_{v_{\text{m}}\cos(\delta_{\text{p}})},\\
&Y^{(i)}_{v_{\text{m}}n_{\text{P}}},\ Y^{(i)}_{r\cos(\delta_{\text{s}})},\ Y^{(i)}_{r\cos(\delta_{\text{p}})},\ Y^{(i)}_{rn_{\text{P}}},\ Y^{(i)}_{\sin(\delta_{\text{s}})\cos(\delta_{\text{s}})},\\
&Y^{(i)}_{\sin(\delta_{\text{s}})\cos(\delta_{\text{p}})},\ Y^{(i)}_{\sin(\delta_{\text{s}})n_{\text{P}}},\ Y^{(i)}_{\cos(\delta_{\text{s}})\sin(\delta_{\text{p}})},\\
&Y^{(i)}_{\sin(\delta_{\text{p}})\cos(\delta_{\text{p}})},\ Y^{(i)}_{\sin(\delta_{\text{p}})n_{\text{P}}},\\
&Y^{(i)}_{uuv_{\text{m}}},\ Y^{(i)}_{v_{\text{m}}v_{\text{m}}v_{\text{m}}},\ Y^{(i)}_{uur},\ Y^{(i)}_{v_{\text{m}}|v_{\text{m}}|r},\ Y^{(i)}_{v_{\text{m}}r|r|},\ Y^{(i)}_{rrr},\\
&Y^{(i)}_{uu\sin(\delta_{\text{s}})},\ Y^{(i)}_{v_{\text{m}}|v_{\text{m}}|\sin(\delta_{\text{s}})},\ Y^{(i)}_{v_{\text{m}}r\sin(\delta_{\text{s}})},\ Y^{(i)}_{r|r|\sin(\delta_{\text{s}})},\\
&Y^{(i)}_{uv_{\text{m}}\cos(\delta_{\text{s}})},\ Y^{(i)}_{ur\cos(\delta_{\text{s}})},\ Y^{(i)}_{u\sin(\delta_{\text{s}})\cos(\delta_{\text{s}})},\\
&Y^{(i)}_{v_{\text{m}}\cos(\delta_{\text{s}})\cos(\delta_{\text{s}})},\ Y^{(i)}_{r\cos(\delta_{\text{s}})\cos(\delta_{\text{s}})},\\
&Y^{(i)}_{\sin(\delta_{\text{s}})\cos(\delta_{\text{s}})\cos(\delta_{\text{s}})},\ Y^{(i)}_{uu\sin(\delta_{\text{p}})},\ Y^{(i)}_{u\cos(\delta_{\text{s}})\sin(\delta_{\text{p}})},\\
&Y^{(i)}_{v_{\text{m}}|v_{\text{m}}|\sin(\delta_{\text{p}})},\ Y^{(i)}_{v_{\text{m}}r\sin(\delta_{\text{p}})},\ Y^{(i)}_{v_{\text{m}}\sin(\delta_{\text{s}})\sin(\delta_{\text{p}})},\\
&Y^{(i)}_{r|r|\sin(\delta_{\text{p}})},\ Y^{(i)}_{r\sin(\delta_{\text{s}})\sin(\delta_{\text{p}})},\ Y^{(i)}_{\cos(\delta_{\text{s}})\cos(\delta_{\text{s}})\sin(\delta_{\text{p}})},\\
&Y^{(i)}_{uv_{\text{m}}\cos(\delta_{\text{p}})},\ Y^{(i)}_{ur\cos(\delta_{\text{p}})},\ Y^{(i)}_{u\sin(\delta_{\text{s}})\cos(\delta_{\text{p}})},\\
&Y^{(i)}_{u\sin(\delta_{\text{p}})\cos(\delta_{\text{p}})},\ Y^{(i)}_{v_{\text{m}}\cos(\delta_{\text{s}})\cos(\delta_{\text{p}})},\ Y^{(i)}_{r\cos(\delta_{\text{s}})\cos(\delta_{\text{p}})},\\
&Y^{(i)}_{\sin(\delta_{\text{s}})\cos(\delta_{\text{s}})\cos(\delta_{\text{p}})},\ Y^{(i)}_{\cos(\delta_{\text{s}})\sin(\delta_{\text{p}})\cos(\delta_{\text{p}})},\ Y^{(i)}_{uv_{\text{m}}n_{\text{P}}},\\
&Y^{(i)}_{urn_{\text{P}}},\ Y^{(i)}_{u\sin(\delta_{\text{s}})n_{\text{P}}},\ Y^{(i)}_{u\sin(\delta_{\text{p}})n_{\text{P}}},\ Y^{(i)}_{v_{\text{m}}\cos(\delta_{\text{s}})n_{\text{P}}},\\
&Y^{(i)}_{v_{\text{m}}\cos(\delta_{\text{p}})n_{\text{P}}},\ Y^{(i)}_{v_{\text{m}}n_{\text{P}}n_{\text{P}}},\ Y^{(i)}_{r\cos(\delta_{\text{s}})n_{\text{P}}},\ Y^{(i)}_{r\cos(\delta_{\text{p}})n_{\text{P}}},\\
&Y^{(i)}_{rn_{\text{P}}n_{\text{P}}},\ Y^{(i)}_{\sin(\delta_{\text{s}})\cos(\delta_{\text{s}})n_{\text{P}}},\ Y^{(i)}_{\sin(\delta_{\text{s}})\cos(\delta_{\text{p}})n_{\text{P}}},\\
&Y^{(i)}_{\sin(\delta_{\text{s}})n_{\text{P}}n_{\text{P}}},\ Y^{(i)}_{\cos(\delta_{\text{s}})\sin(\delta_{\text{p}})n_{\text{P}}},\ Y^{(i)}_{\sin(\delta_{\text{p}})\cos(\delta_{\text{p}})n_{\text{P}}},\\
&Y^{(i)}_{\sin(\delta_{\text{p}})n_{\text{P}}n_{\text{P}}}\big)
\end{aligned}
\tag{15}
$$

$$
\begin{aligned}
z_{\mathrm{odd}} = \big(&v_{\mathrm{m}},\ r,\ \sin(\delta_{\mathrm{s}}),\ \sin(\delta_{\mathrm{p}}),\ uv_{\mathrm{m}},\ ur,\ u\sin(\delta_{\mathrm{s}}),\\
&u\sin(\delta_{\mathrm{p}}),\ v_{\mathrm{m}}\cos(\delta_{\mathrm{s}}),\ v_{\mathrm{m}}\cos(\delta_{\mathrm{p}}),\ v_{\mathrm{m}}n_{\mathrm{P}},\\
&r\cos(\delta_{\mathrm{s}}),\ r\cos(\delta_{\mathrm{p}}),\ rn_{\mathrm{P}},\ \sin(\delta_{\mathrm{s}})\cos(\delta_{\mathrm{s}}),\\
&\sin(\delta_{\mathrm{s}})\cos(\delta_{\mathrm{p}}),\ \sin(\delta_{\mathrm{s}})n_{\mathrm{P}},\ \cos(\delta_{\mathrm{s}})\sin(\delta_{\mathrm{p}}),\\
&\sin(\delta_{\mathrm{p}})\cos(\delta_{\mathrm{p}}),\ \sin(\delta_{\mathrm{p}})n_{\mathrm{P}},\\
&uuv_{\mathrm{m}},\ v_{\mathrm{m}}v_{\mathrm{m}}v_{\mathrm{m}},\ uur,\ v_{\mathrm{m}}|v_{\mathrm{m}}|r,\ v_{\mathrm{m}}r|r|,\ rrr,\\
&uu\sin(\delta_{\mathrm{s}}),\ v_{\mathrm{m}}|v_{\mathrm{m}}|\sin(\delta_{\mathrm{s}}),\ v_{\mathrm{m}}r\sin(\delta_{\mathrm{s}}),\\
&r|r|\sin(\delta_{\mathrm{s}}),\ uv_{\mathrm{m}}\cos(\delta_{\mathrm{s}}),\ ur\cos(\delta_{\mathrm{s}}),\\
&u\sin(\delta_{\mathrm{s}})\cos(\delta_{\mathrm{s}}),\ v_{\mathrm{m}}\cos(\delta_{\mathrm{s}})\cos(\delta_{\mathrm{s}}),\\
&r\cos(\delta_{\mathrm{s}})\cos(\delta_{\mathrm{s}}),\ \sin(\delta_{\mathrm{s}})\cos(\delta_{\mathrm{s}})\cos(\delta_{\mathrm{s}}),\\
&uu\sin(\delta_{\mathrm{p}}),\ u\cos(\delta_{\mathrm{s}})\sin(\delta_{\mathrm{p}}),\ v_{\mathrm{m}}|v_{\mathrm{m}}|\sin(\delta_{\mathrm{p}}),\\
&v_{\mathrm{m}}r\sin(\delta_{\mathrm{p}}),\ v_{\mathrm{m}}\sin(\delta_{\mathrm{s}})\sin(\delta_{\mathrm{p}}),\ r|r|\sin(\delta_{\mathrm{p}}),\\
&r\sin(\delta_{\mathrm{s}})\sin(\delta_{\mathrm{p}}),\ \cos(\delta_{\mathrm{s}})\cos(\delta_{\mathrm{s}})\sin(\delta_{\mathrm{p}}),\\
&uv_{\mathrm{m}}\cos(\delta_{\mathrm{p}}),\ ur\cos(\delta_{\mathrm{p}}),\ u\sin(\delta_{\mathrm{s}})\cos(\delta_{\mathrm{p}}),\\
&u\sin(\delta_{\mathrm{p}})\cos(\delta_{\mathrm{p}}),\ v_{\mathrm{m}}\cos(\delta_{\mathrm{s}})\cos(\delta_{\mathrm{p}}),\\
&r\cos(\delta_{\mathrm{s}})\cos(\delta_{\mathrm{p}}),\ \sin(\delta_{\mathrm{s}})\cos(\delta_{\mathrm{s}})\cos(\delta_{\mathrm{p}}),\\
&\cos(\delta_{\mathrm{s}})\sin(\delta_{\mathrm{p}})\cos(\delta_{\mathrm{p}}),\ uv_{\mathrm{m}}n_{\mathrm{P}},\ urn_{\mathrm{P}},\\
&u\sin(\delta_{\mathrm{s}})n_{\mathrm{P}},\ u\sin(\delta_{\mathrm{p}})n_{\mathrm{P}},\ v_{\mathrm{m}}\cos(\delta_{\mathrm{s}})n_{\mathrm{P}},\\
&v_{\mathrm{m}}\cos(\delta_{\mathrm{p}})n_{\mathrm{P}},\ v_{\mathrm{m}}n_{\mathrm{P}}n_{\mathrm{P}},\ r\cos(\delta_{\mathrm{s}})n_{\mathrm{P}},\\
&r\cos(\delta_{\mathrm{p}})n_{\mathrm{P}},\ rn_{\mathrm{P}}n_{\mathrm{P}},\ \sin(\delta_{\mathrm{s}})\cos(\delta_{\mathrm{s}})n_{\mathrm{P}},\\
&\sin(\delta_{\mathrm{s}})\cos(\delta_{\mathrm{p}})n_{\mathrm{P}},\ \sin(\delta_{\mathrm{s}})n_{\mathrm{P}}n_{\mathrm{P}},\\
&\cos(\delta_{\mathrm{s}})\sin(\delta_{\mathrm{p}})n_{\mathrm{P}},\ \sin(\delta_{\mathrm{p}})\cos(\delta_{\mathrm{p}})n_{\mathrm{P}},\\
&\sin(\delta_{\mathrm{p}})n_{\mathrm{P}}n_{\mathrm{P}}\big).
\end{aligned}
\tag{16}
$$

$N^{(i)}$ is omitted because it is similar to Eq. 15. 2nd-order model consists only with linear and 2nd-order term of Eqs 13, 15, 14, 16. Here, the superscript i represents the ith parameter set of the coefficient vector Submodel, described in the following section.

2.2.3 Submodel

The proposed model uses the same polynomial formulae for all operational conditions but changes the values of the hydrodynamic coefficients for each condition, to achieve both simplicity of the derivation and complexity of the model, as described in Idea 2. The complexity of the model can be increased arbitrarily by increasing the number of conditional branches. Here, we named the value set of coefficients for each condition as "Submodel". In our previous study [35], a mathematical model of a single-propeller, single-rudder ship was developed with a Submodel for each propeller operating quadrant (defined by u, n_p). Since the subject ship of the current study has a VecTwin rudder, the propeller is always in forward rotation. Therefore, the simplest Submodel would be Submodel-2, which switches by the sign of u. The conditional branch of Submodel-2 is shown in Algorithm 1.

Algorithm 1 $X^{(i)}$ of Submodel-2

```
if u ≥ 0 then
    X^(i) = X^(1)
else
    X^(i) = X^(2)
end if
```

Here, algorithm 1 shows only $\boldsymbol{X}^{(i)}$, but switches $\boldsymbol{Y}^{(i)}$, $\boldsymbol{N}^{(i)}$ as well.

VecTwin rudder-equipped vessels do not reverse their propellers but instead gain stopping power by taking a large rudder angle up to 105°. Therefore, we can add a conditional branch with a nominal stall angle of rudders. The VecTwin rudders have a nominal stall angle of $\alpha_{\mathrm{stall,s}} = 50°$, $\alpha_{\mathrm{stall,p}} = 55°$ which can be observed from the captive model test results [44]. Submodel-3 is shown in Algorithm 2 and Submodel-4 shown in Algorithm 3. Submodel-3 uses the stall angle as the branch for forwarding conditions only, but Submodel-4 uses it for both forward and astern.

Algorithm 2 $X^{(i)}$ of Submodel-3

```
if u ≥ 0 then
    if |δ_s| < α_stall,s and |δ_s| < α_stall,p then
        X^(i) = X^(1)
    else
        X^(i) = X^(2)
    end if
else
    X^(i) = X^(3)
end if
```

Algorithm 3 $X^{(i)}$ of Submodel-4

```
if u ≥ 0 then
    if |δ_s| < α_stall,s and |δ_s| < α_stall,p then
        X^(i) = X^(1)
    else
        X^(i) = X^(2)
    end if
else
    if |δ_s| < α_stall,s and |δ_s| < α_stall,p then
        X^(i) = X^(3)
    else
        X^(i) = X^(4)
    end if
end if
```

As shown above, the proposed model can apply to various kind of motions by adding Submodels because it includes all terms that may be relevant to the characteristics of the flow and actuators. For example, for a single-propeller,

single-rudder ship, if the user assumes that characteristics of propeller reversal are not crucial for their use, then Submodel-2 can be used. Still, if a difference is desired, Submodel-4 can be used.

2.3 Modeling on wind disturbance

In this study, the wind force is modeled using Fujiwara's regression formula, [38], which has fewer model parameters than Isherwood's regression [45] because trigonometric functions represent wind direction. Fujiwara's wind force model is shown by Eq. 17,

$$\begin{aligned} X_A &= (1/2)\rho_A U_A^2 A_T \cdot C_X \\ Y_A &= (1/2)\rho_A U_A^2 A_L \cdot C_Y \\ N_A &= (1/2)\rho_A U_A^2 A_L L_{OA} \cdot C_N, \end{aligned} \tag{17}$$

where

$$\begin{aligned} C_X =& X_{A0} + X_{A1}\cos(2\pi - \gamma_A) + X_{A3}\cos 3(2\pi - \gamma_A) \\ &+ X_{A5}\cos 5(2\pi - \gamma_A) \\ C_Y =& Y_{A1}\sin(2\pi - \gamma_A) + Y_{A3}\sin 3(2\pi - \gamma_A) \\ &+ Y_{A5}\sin 5(2\pi - \gamma_A) \\ C_N =& N_{A1}\sin(2\pi - \gamma_A) + N_{A2}\sin 2(2\pi - \gamma_A) \\ &+ N_{A3}\sin 3(2\pi - \gamma_A). \end{aligned} \tag{18}$$

X_{Ai}, Y_{Ai}, N_{Ai} are the model coefficients of wind force. Fujiwara's formula estimates the X_{Ai}, Y_{Ai}, N_{Ai} by regression formulae with the ship's particulars as explanatory variables. But in this study, they were obtained by optimization.

3 Optimization procedure and its condition

In this chapter, we describe the method to optimize the parameters of a proposed model using system identification (SI). SI of ship maneuvering is defined as the problem of finding a parameter vector of an optimal mathematical model $\boldsymbol{\theta}_{\text{opt}}$ that minimizes the difference between the state variable history of the input dataset $\mathcal{D}$ and the state variable history estimated by the maneuvering simulation using obtained model. Here, $\mathcal{D}$ is the measured results of model tests or full-scale ship trials and includes the data of state variables $\boldsymbol{s}_t$, control input $\boldsymbol{a}_t$ and disturbances $\boldsymbol{\omega}_t$. The dataset $\mathcal{D}$ consisted of a training dataset $\mathcal{D}^{(\text{train})}$ for the optimization procedure, validation dataset $\mathcal{D}^{(\text{validation})}$ for selecting the optimal parameter and hyperparameter, and test dataset $\mathcal{D}^{(\text{test})}$ to test the generalization performance on unknown data. From now on, bracketed superscripts indicate values for the associated dataset, and superscript (input) indicates one of (train), (validation), or (test).

Hereafter, the chapter will be organized as follows: the objective function, which is the metric for the optimization, is described in Sect. 3.1; the domain of the parameter exploration is described in Sect. 3.2; the details of the dataset are described in Sect. 3.3; the hyperparameters are described in Sect. 3.4; the optimization algorithm CMA-ES in Sect. 3.5; and a model generated by conventional parameter identification method used as a comparison is described in Sect. 3.6.

3.1 Objective function

The optimization procedure is defined as exploration for the parameter vector $\boldsymbol{\theta}$ of the model that minimizes the objective function $\mathcal{F}$ for the training data set $\mathcal{D}^{(\text{train})}$ using an optimization algorithm, CMA-ES. Objective function $\mathcal{F}$ is defined as follows:

$$\boldsymbol{\theta}_{\text{opt}}^{(\text{train})} = \underset{\boldsymbol{\theta}\in\Theta}{\operatorname{argmin}}\, \mathcal{F}(\boldsymbol{\theta}; \mathcal{D}^{(\text{train})}) \tag{19}$$

where

$$\begin{aligned} \mathcal{F}(\boldsymbol{\theta}; \mathcal{D}^{(\text{train})}) =& \mathcal{L}^{(\text{train})}(\boldsymbol{\theta}; \mathcal{D}^{(\text{train})}) \\ &+ \alpha P_{\text{div}}(\boldsymbol{\theta}) + \lambda\|\boldsymbol{\theta}\|_1 \end{aligned} \tag{20}$$

$$\begin{aligned} &\mathcal{L}^{(\text{train})}(\boldsymbol{\theta}; \mathcal{D}^{(\text{train})}) \\ &\quad = \sum_{i=1}^{N} \int_{t=0}^{t_{\text{f}}} \|\hat{\boldsymbol{s}}_t^{(\text{train},i)} - \hat{\boldsymbol{s}}_t^{(\text{sim},i)}(\boldsymbol{\theta})\|^2 \mathrm{d}t. \end{aligned} \tag{21}$$

The first term of Eq. 20 is the error norm $\mathcal{L}$ of the maneuvering simulation using $\boldsymbol{\theta}$ for the data set $\mathcal{D}^{(\text{train})}$. The second term is the deviation penalty from the a priori acceleration range for $\boldsymbol{\theta}$, and α is its weighting coefficient. The third term is the regularization term, and λ is the L1 regularization penalty. Detail of the first term is described in Sect. 3.1.1, and the second term is described in Sect. 3.1.2. In Eq. 21, superscript $i = 1 \cdots N$ denotes the ith contiguous subsequences (CS), and N denotes the total number of CS. Details of CS are stated in the next subsection. Also, $\hat{s}_{t,j}^{(\cdot,i)}$ is the standardized state variables of the ith CS at time t, and their jth component is defined by the mean $\mu_j^{(\text{train},i)}$ and standard deviation $\sigma_j^{(\text{train},i)}$ as in the following equation:

$$\hat{s}_{t,j}^{(\text{train},i)} = \left(s_{t,j}^{(\text{train},i)} - \mu_j^{(\text{train},i)}\right)/\sigma_j^{(\text{train},i)} \tag{22}$$

$$\hat{s}_{t,j}^{(\text{sim},i)} = \left(s_{t,j}^{(\text{sim},i)} - \mu_j^{(\text{train},i)}\right)/\sigma_j^{(\text{train},i)}. \tag{23}$$

3.1.1 Maneuvering simulation and error norm $\mathcal{L}$

The maneuvering simulation is conducted to evaluate the performance of $\boldsymbol{\theta}$, by estimating the state variable $\boldsymbol{s}_t^{(\mathrm{sim})}$ as an initial value problem using the mathematical model described in Sect. 2 and $\boldsymbol{\theta}$. The control input $\boldsymbol{a}_t$ and the disturbance $\boldsymbol{\omega}_t$ are given. In this study, $\boldsymbol{s}_{t_0}^{(\mathrm{sim})}$, $\boldsymbol{a}_t^{(\mathrm{sim})}$, $\boldsymbol{\omega}_t^{(\mathrm{sim})}$ were defined by the input dataset $\mathcal{D}^{(\mathrm{input})}$ as Eq. 24:

$$\begin{aligned}\boldsymbol{s}_{t_0}^{(\mathrm{sim},i)} &= \boldsymbol{s}_{t_0}^{(\mathrm{input},i)}\\ \boldsymbol{a}_t^{(\mathrm{sim})} &= \boldsymbol{a}_t^{(\mathrm{input},i)}\\ \boldsymbol{\omega}_t^{(\mathrm{sim},i)} &= \boldsymbol{\omega}_t^{(\mathrm{input},i)}.\end{aligned} \tag{24}$$

Here, $\mathcal{D}^{(\mathrm{input})}$ is one of $\mathcal{D}^{(\mathrm{train})}$, $\mathcal{D}^{(\mathrm{validation})}$, $\mathcal{D}^{(\mathrm{test})}$. We can get the time derivative of $\boldsymbol{s}_t$: $\dot{\boldsymbol{s}}_t \equiv (\dot{u},\ \dot{v_{\mathrm{m}}},\ \dot{r})$ by solving Eq. 1. The first-order Euler method was used for time development. The time interval $\Delta t = 0.1$ s was used.

In the simulation, we divide $\mathcal{D}^{(\mathrm{input})}$ into contiguous subsequences: $\mathcal{D}^{(\mathrm{input},i)}$ to avoid accumulation of errors. We divided $\mathcal{D}^{(\mathrm{input})}$ into CS because the velocity was used in the error norm (Eq. 21) instead of accelerations. Accelerations can be directly obtained by solving Eq. 1; however, acceleration measurement is more difficult than speed and angular velocity measurement. On the other hand, the estimation error of accelerations will be accumulated in the velocity components. The length of the CS is set to $t_{\mathrm{f}} = 100$ s.

In addition, because we search for coefficients from a wide range, certain combinations of model coefficients can result in unusually large acceleration during maneuvering simulations. Unrealistically, large acceleration will cause numerical overflows in $\boldsymbol{s}_t$ or $\mathcal{L}$. We try to prevent overflow by substituting the extra large value with a constant value corresponding to the time-step number when the absolute values of velocity and acceleration exceed the limit $\boldsymbol{S}_{\mathrm{limit}}$, same as [1]:

$$S_{t,j=1\ldots6}(t) = \begin{cases} \mathrm{sgn}\left(S_{t,j}\right)(2 - t/t_{\mathrm{f}})S_{\mathrm{limit},j} & : |S_{t,j}| > S_{\mathrm{limit},j} \\ S_{t,j} & : \text{else} \end{cases} \tag{25}$$

where

$$\boldsymbol{S}_t \equiv (\boldsymbol{s}_t, \dot{\boldsymbol{s}}_t) \tag{26}$$

$$\begin{aligned}\boldsymbol{S}_{\mathrm{limit}} &= (a,\ a,\ 2a/L_{\mathrm{pp}},\ a,\ a,\ 2a/L_{\mathrm{pp}})\\ a &= 1.0 \times 10^{80}\end{aligned} \tag{27}$$

$$\mathrm{sgn}(x) = \begin{cases} 1 & : x > 0 \\ -1 & : x < 0 \\ 0 & : x = 0 \end{cases}. \tag{28}$$

3.1.2 Deviation penalty P_{div}

Because the proposed model is a simple polynomial equation that does not include hydrodynamic constraints, the acceleration may be overestimated for unknown data, which may cause generalization performance degradation. To prevent overestimation, we imposed a penalty on the objective function when the estimated acceleration exceeded the a priori limit for a specific state and control inputs, which was assumed to give maximum acceleration. This method [46] was expected to eliminate model parameters that return unrealistic accelerations.

Below is the detailed calculation method of the deviation penalty, P_{div}. With given initial state variable $\boldsymbol{s}_0$, steady control input $\boldsymbol{a}_t = \boldsymbol{a}_0$, and steady disturbance $\boldsymbol{\omega}_t = \boldsymbol{\omega}_0$ a penalty is applied if the estimated acceleration $\dot{\boldsymbol{s}}_t^{(\mathrm{sim})}$ exceed the predefined range $\left[\dot{\boldsymbol{s}}_{\min}, \dot{\boldsymbol{s}}_{\max}\right]$ as follows:

$$P_{\mathrm{div}} = \sum_{n=1}^{N_{\mathrm{div}}} P_n \tag{29}$$

where

$$P_n = \begin{cases} 1 - \frac{t_{\mathrm{over}} - \Delta t}{t_{\mathrm{f}}} & : t_{\mathrm{over}} < t_{\mathrm{f}}^{(\mathrm{div})} \\ 0 & : \text{else} \end{cases} \tag{30}$$

$$t_{\mathrm{over}} = \inf\left\{ t \geq 0 : \dot{\boldsymbol{s}}_t^{(\mathrm{sim})} \notin \left[\dot{\boldsymbol{s}}_{\min}, \dot{\boldsymbol{s}}_{\max}\right] \right\}. \tag{31}$$

Here $t_{\mathrm{f}}^{(\mathrm{div})}$ is duration of the maneuvering simulation and $t_{\mathrm{f}} = 1$ s. Since $\boldsymbol{s}_0$ and $\boldsymbol{a}_0$ are expected combinations to generate the maximum or minimum acceleration, we set $s_0 = (u_0,\ v_0,\ r_0)$ by the maximum and minimum value of $\mathcal{D}$ with a certain margin, and set $a_0 = (n_{\mathrm{P0}},\ \delta_{s0},\ \delta_{p0})$ by the value which expected to generate maximum and minimum control forces. Accordingly, $\boldsymbol{s}_0$ and $\boldsymbol{a}_0$ are show as in Eq. 32:

$$\begin{aligned} u_0 &\in \{-0.2, 0.0, 0.5\}\\ v_0 &\in \{-0.2, 0.0, 0.2\}\\ r_0 &\in \{-0.1, 0.0, 0.1\}\\ n_{\mathrm{P0}} &\in \{0.0, 12.5\}\\ \delta_{s0} &\in \{-35, 0, 45, 60, 90\}\\ \delta_{p0} &\in \{35, 0, -45, -60, -90\}. \end{aligned} \tag{32}$$

Total number of combination N_{div} is 1350. In addition, no wind disturbance is assumed $\boldsymbol{\omega}_0 = (0,\ 0)$.

The range of $\left[\dot{\boldsymbol{s}}_{\min}, \dot{\boldsymbol{s}}_{\max}\right]$ was defined using a priori information. Here, we used 1-second moving average of the numerical differentiation of $\boldsymbol{s}_t^{(\mathcal{D})}$ as the acceleration $\dot{\boldsymbol{s}}_t^{(\mathcal{D})}$. This study's model experiment did not measure acceleration due to its low signal-noise ratio. The 99.7th percentile

of the of modulus of the acceleration $\boldsymbol{Q}_{99.7}(|\dot{\boldsymbol{s}}_t^{(\mathcal{D})}|)$ was used to set the range:

$$\left[\dot{\boldsymbol{s}}_{\min}, \dot{\boldsymbol{s}}_{\max}\right] = [-\boldsymbol{Q}_{99.7}(|\dot{\boldsymbol{s}}_t^{(\mathcal{D})}|),\ \boldsymbol{Q}_{99.7}(|\dot{\boldsymbol{s}}_t^{(\mathcal{D})}|)]. \tag{33}$$

We can simplify the range by employing the modulus function in Eq. 33. The reason for using the 99.7th percentile is to remove the effect of noise amplified by numerical differentiation. If the subject ship's acceleration can be measured appropriately, measured acceleration is more suitable.

3.2 Exploration domain

In this section, we show the exploration domain $\boldsymbol{\Theta}$ of parameter $\boldsymbol{\theta}$. The parameter vector $\boldsymbol{\theta}$ consists of added masses and inertia, hydrodynamic coefficients, and wind force coefficients as follows:

$$\begin{aligned}\boldsymbol{\theta} = \big(&m_x,\ m_y,\ I_{zz} + J_{zz},\\ &\boldsymbol{X}^{(i)},\ \boldsymbol{Y}^{(i)},\ \boldsymbol{N}^{(i)},\\ &X_{A0},\ X_{A1},\ X_{A3},\ X_{A5},\\ &Y_{A1},\ Y_{A3},\ Y_{A5},\ N_{A1},\ N_{A2},\ X_{A3}\ \big).\end{aligned} \tag{34}$$

Domain $\boldsymbol{\Theta}$ must be defined without a captive model test of the subject ship a priori. In our previous study [1], boundary of the domain $\boldsymbol{\Theta}$ is set to be approximately 10 times greater value of a priori solutions, i.e., captive model test results and empirical value. Because of this vast exploration domain, we believed we could obtain optimal coefficients even if the hull form or model's formulae differed from a priori solutions. Hence, we set the domain boundary by multiplying the coefficient values of the classic Abkowitz model for single-propeller, single-rudder ship [3]:

$$\theta_j \in \Theta_j = \big[-1.0, 1.0\big]. \tag{35}$$

Here, Θ_j is a domain for the j-th component of the parameter vector. Moreover, several exceptions of domain boundary setting were made like the previous study as follows:

- Maximum value of $X_u,\ X_{uu},\ Y_{v_\mathrm{m}},\ N_r$ are set to 0 because the signs of diagonal resistance components are self-explanatory.
- Minimum value of X_{n_P} was set to 0 because the sign of the first-order thrust coefficient is self-explanatory.
- We multiplied 10 to Eq. 35 according to the order of r contained in θ_j, because r is relatively smaller than the other components of $\boldsymbol{x}$ due to its radian/s dimension.
- We multiplied 0.1 to Eq. 35 according to the order of n_P contained in θ_j, because the subject ship is a model ship, n_P is relatively larger than the other components of $\boldsymbol{x}$.
- The added mass, added mass moment, and wind force coefficients were determined from the empirical value $\theta_{\mathrm{empirical},j}$. For $m_x,\ m_y,\ I_{zz} + J_{zz}$, $\Theta_j = \big[-10\theta_{\mathrm{empirical},j},\ 10\theta_{\mathrm{empirical},j}\big]$ and for wind coefficient, $\Theta_j = \big[-10\theta_{\mathrm{empirical},j},\ 10\theta_{\mathrm{empirical},j}\big]$.

There are pros and cons to searching dimensional values. In dimensional form, domain $\boldsymbol{\Theta}$ depends on the ship's size; hence, $\boldsymbol{\Theta}$ needs to be determined by repeated trials every time the subject ship changes. In contrast, $\boldsymbol{\Theta}$ for non-dimensional coefficients can set its domain boundaries independent of the size and scale of the ship; however, non-dimensionalization causes a problem when ship speed is zero. Further study on domain design is needed.

3.3 Dataset

This section describes the datasets used in the study. Maneuvering time histories of a 3-meter free-running model ship were used as the datasets. Principal particulars of the subject model ship are shown on Table 1. The measurement system of the model ship is almost the same as in the previous study [1], with the following differences. Ship speed u and v_m were calculated from speed over ground (SOG), course over ground (COG) measured by the GNSS receiver, and ship heading measured by fiber optical gyro (FOG). In addition, compared to previous studies, the current FOG has better heading accuracy; the yaw drift was about 1°/hour. Moreover, unlike in previous studies, r was not filtered due to the improved performance of FOG.

Random maneuvers are the maneuvers used in the dataset, same as the previous study [1]. The reason for using random maneuvers was used to ensure the stability of the model (Requirement 7), as described in Sect. 2. The random maneuvers are intended to obtain various different values of state variables and control inputs that can occur as the motion of the subject ship as possible. In this study, as in the previous studies, the model ship operator gives random $\boldsymbol{a}_t$ so that the state variables and control inputs are distributed. For details on the random maneuvers, please refer to the previous study [1]. The experiment was conducted in an experiment pond (*Inukai* Pond) at Osaka University. Water depth was sufficiently deep enough to neglect shallow water effect.

The control input $\boldsymbol{a}_t$ of random maneuvers was given within a set upper and lower limit range as shown in Table 3. The range of $\delta_\mathrm{s},\ \delta_\mathrm{p}$ is the maximum mechanical steering range of the VecTwin rudder. With the maximum propeller speed $n_{\mathrm{p\,max}}$, the ship reaches $u \approx 0.6$ m/s in a forwarding equilibrium state. The dimensionless speed corresponding to $u = 0.6$ is $\mathrm{Fr} = u/\sqrt{gL_\mathrm{pp}} = 0.11$, equivalent to 6.7 knots for a medium-sized ship (assuming $L_\mathrm{pp} = 100$ m). Therefore, $n_{\mathrm{p\,max}}$ is a typical range of propeller speed for ship handling in a harbor. Since the subject ship is equipped with VecTwin

rudder system, the ship can stop and astern without reversing the propeller; hence, $n_{\mathrm{p\,min}} = 0$ was used.

The entire dataset $\mathcal{D}$ was divided into $\mathcal{D}^{(\mathrm{train})}$, $\mathcal{D}^{(\mathrm{validation})}$ and $\mathcal{D}^{(\mathrm{test})}$, and here we compare the distribution among the datasets. First, the number of samples for each dataset is shown in time in Table 2. The measurement frequency of the datasets is 0.1 s, equal to Δt of the maneuvering simulation. The entire dataset $\mathcal{D}$ is divided to be the length of each dataset $T^{(\mathrm{train})}$, $T^{(\mathrm{validation})}$, $T^{(\mathrm{test})}$ is approximately 6 : 1 : 1. The distribution of $\boldsymbol{s}_t$ and control inputs n_{P}, $\delta_{\mathrm{s}}, \delta_{\mathrm{p}}$ for each dataset are shown in Fig. 2. The distributions of the datasets generally agree well with each other.

The data set $\mathcal{D}$ is expected to cover all possible maneuvers that may occur during harbor maneuvers, including unknown maneuvers, to obtain a robust model. There is no clear definition of the range of state variables for harbor maneuvers; however, the state variables in $\mathcal{D}$ are comparable to the empirical range of speeds used in the harbor when converted to real ship scale. Specifically, u is $u \in [-0.1,\ 0.4]$, equivalent to 1.2 knots astern and 4.5 knots forward of $L_{\mathrm{pp}} = 100$. Both v_{m} and r are approximately symmetric, i.e., positively and negatively symmetrically distributed, and $v_{\mathrm{m}} \in [-0.1,\ 0.1]$, which is the range of slow maneuver corresponding to $\mathrm{Fr}_{v_{\mathrm{m}}} = \pm 0.018$ and 1.2 knots at $L_{\mathrm{pp}} = 100$. Further, by observing the distribution of u and v_{m}, we see that the drift angle β is distributed over the entire circumference.

In addition, random maneuvers are favorable because correlations between state variables and control inputs are weak. The multi-collinearity is a known problem when using zig-zag maneuvers and turnings as training data due to the strong correlation between v_{m} and r in those motions [3, 47]. On the other hand, in the random maneuvers, the correlation between all state variables and control inputs is weak, not only between v_{m} and r as shown in Fig. 2.

In this study, random maneuvers were employed as the data set, but the validity of the proposed model needs to be demonstrated for motions other than random maneuvers. Here, other than random maneuvers, Crash-Astern (CA) test data set $\mathcal{D}^{(\mathrm{CA})}$ was employed. A CA test was performed by making a steady propeller revolution at $n_{\mathrm{P}} = 7.3$ rps or $n_{\mathrm{P}} = 9.8$ rps from a stopped state, accelerating straight ahead at $\delta_{\mathrm{sp}} = 0°$ for 120 s ($n_{\mathrm{P}} = 7.3$) or 100 s ($n_{\mathrm{P}} = 9.8$), and steer $\delta_{\mathrm{s}} = 105°$, $\delta_{\mathrm{p}} = -105°$ to decelerate, stop, and astern. In total, $\mathcal{D}^{(\mathrm{CA})}$ contains four CA tests, and each test is about 400 s. Hence, the total length of the $\mathcal{D}^{(\mathrm{CA})}$ is $T^{(\mathrm{CA})} = 1647.7$ s is shown in Table 2.

The normalized histogram of $\mathcal{D}^{(\mathrm{CA})}$ and $\mathcal{D}^{(\mathrm{train})}$ is shown in Fig. 3. As mentioned earlier, CA test only used a specific n_{P}, δ_{s}, δ_{p} as a command signal, which results in a stronger n_{P}, δ_{s}, δ_{p} bias than the random maneuvers. In addition, since n_{P}, δ_{s}, δ_{p} were constant, the speed developed faster, and the distribution of u was wider than that of random maneuvering. On the other hand, v_{m} and r were more biased around 0 than in random maneuvers.

3.4 Numerical conditions of mathematical models and hyperparameters

The objective function of Eq. 20 requires the user to select the hyperparameters α and λ. The α and λ depend on the model's complexity, i.e., order of the model's polynomials and number of Submodels. In this study, order of polynomials and the number of Submodels were calculated for five combinations as shown in Table 4. Hereafter, a model with Submodel-2 and 2nd-order polynomials will be referred to as a "SM-2, 2nd-order model." In addition, hyperparameters α and λ are used for the combinations shown in Tables 5, 6. Hereafter, an optimization performed with a specific model, α, and λ is referred to as a "computational case." A total of 28 computational cases were executed.

3.5 CMA-ES and its conditions

This study used the optimization method Covariance Matrix Adaption-Evolution Strategy (CMA-ES) [48]. CMA-ES is effective for complex optimization problems where the problems are non-separable and multi-modal [49, 50]. In addition, CMA-ES has strong search capability for optimization problems up to several hundred dimensions [51]. We expect CMA-ES to be effective for the Black Box optimization

Table 1 Principal particulars of the subject ship

Parameter	Value
Length between perpendiculars: L_{pp} (m)	3.000
Breadth (m)	0.484
Draft (m)	0.172

Table 2 Duration of datasets

Name	$T^{(\mathrm{train})}$	$T^{(\mathrm{validation})}$	$T^{(\mathrm{test})}$	$T^{(\mathrm{CA})}$
Value (s)	7407.4	1201.2	1201.2	1647.7

Table 3 Maximum and minimum of control input n_{P}, δ_{s}, δ_{p} of random maneuver data set $\mathcal{D}$

Parameter	Maximum and minimum
n_{P} (rps)	[0, 12.5]
δ_{s} (deg.)	[−35, 105]
δ_{p} (deg.)	[−105, 35]

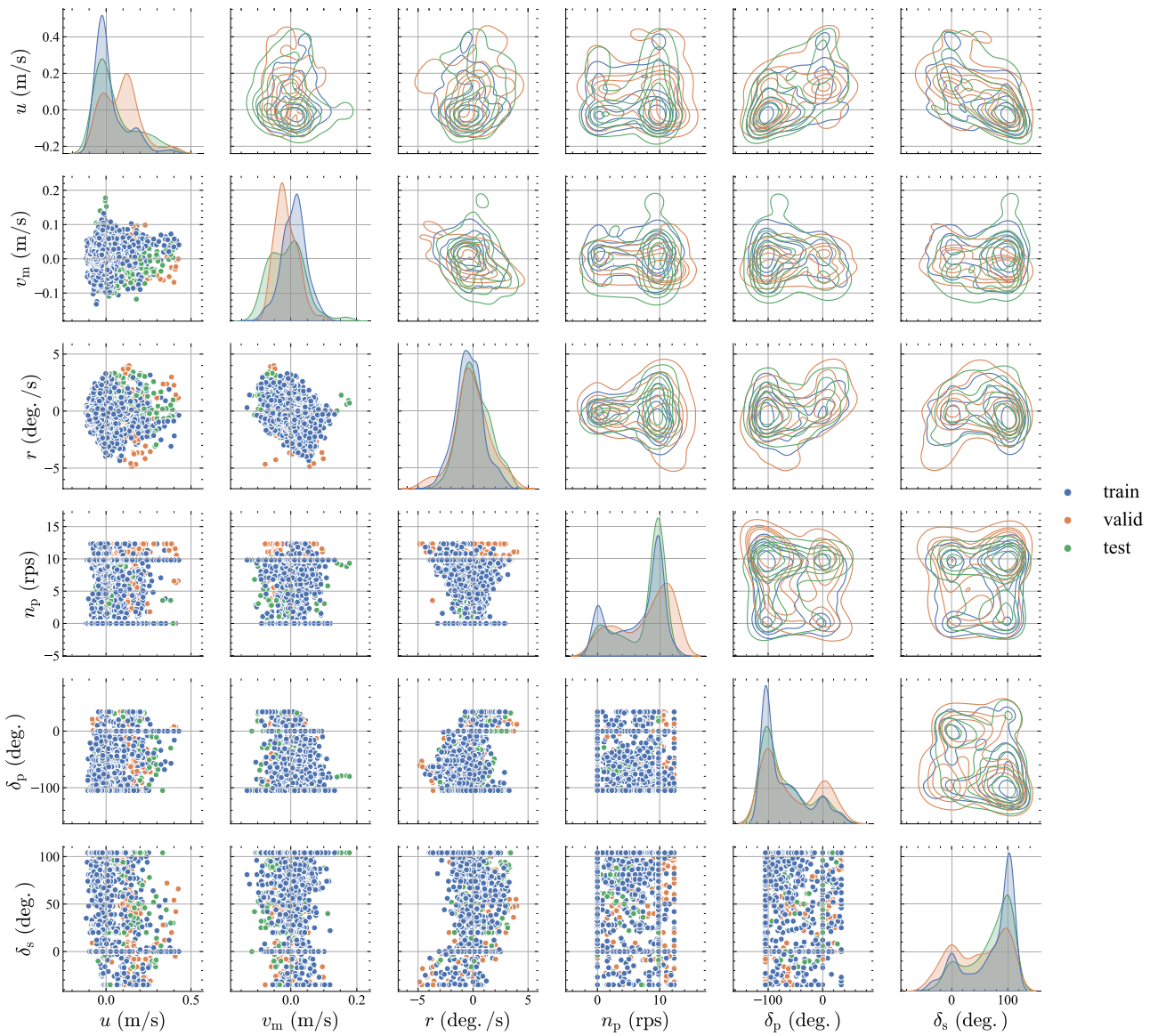

Fig. 2 Distribution of state variables and control inputs of data sets. Diagonal and upper triangle figures are univariate and bivariate kernel density estimations of state variables and control inputs, respectively. Lower triangle figures are bivariable scatter plots of state variables and control inputs. In this figure, data sets were re-sampled with one sample per five seconds for plotting

problem we are tackling in this study. In addition, CMA-ES has a practical advantage in requiring fewer hyperparameters to be determined by the user.

CMA-ES uses the normal distribution to generate candidate solutions and updates the statistics (mean and covariance matrices) of the normal distribution using candidates with a high degree of adaption to the objective function among the candidates. This process of generation, evaluation, and update is iterated, which is interpreted as minimizing the expectation value of the evaluation function [52, 53].

In this study, the CMA-ES with box constraints[54] and the restart strategy [55] was used as in the previous study [1, 35]. The initial and maximum population sizes of candidate solutions were set to 64 and 256, respectively. This study's optimization using CMA-ES was terminated at 5×10^5 iterations.

3.6 Reference model

The proposed model needs to be verified whether it can be used as a maneuvering estimation module of a harbor maneuvering simulator. The authors confirmed the validity of the proposed method by confirming that the proposed model has the same or better estimation performance as the model identified by conventional methods. That is, the

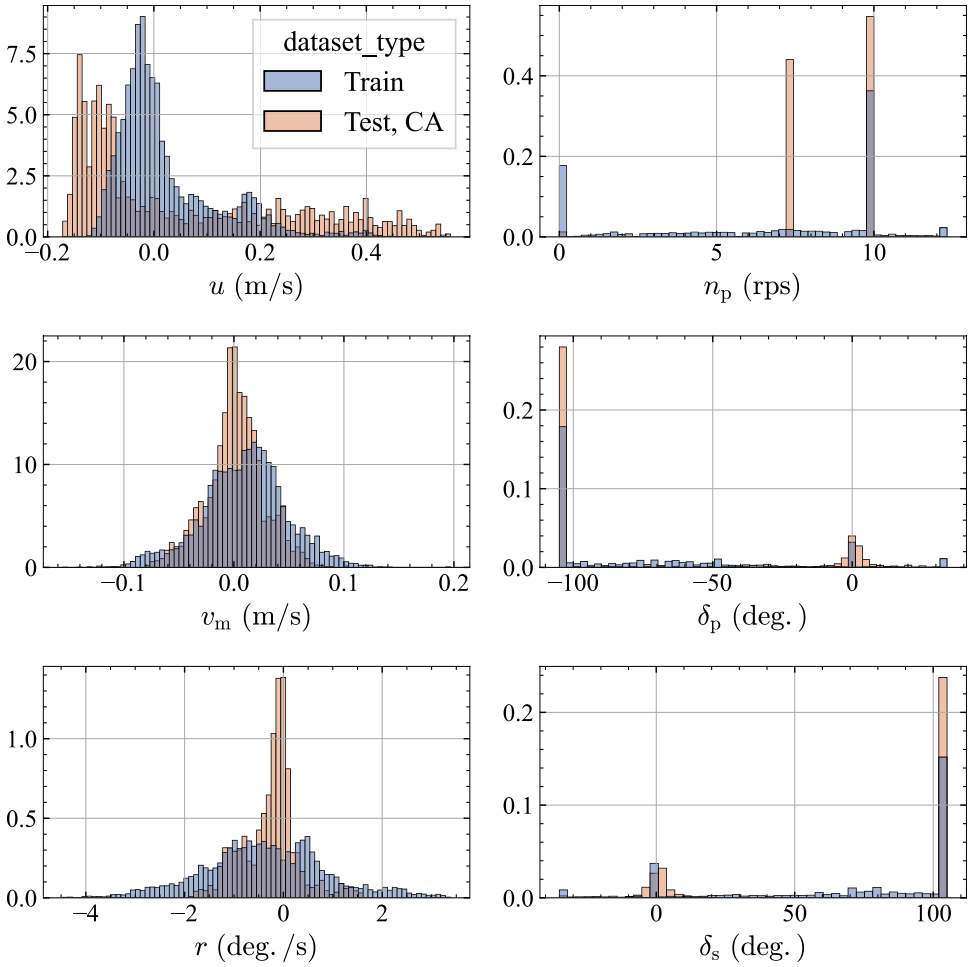

Fig. 3 Histograms of x_k of $\mathcal{D}^{(\mathrm{train})}$ and $\mathcal{D}^{(\mathrm{CA})}$. Histograms are normalized to make the total area of the bins to be 1 for each data set

Table 4 Maximum order of polynomials and number of Submodels of the mathematical models

Submodels	Max. order	Unknown variables
2	2nd order	133
3		193
4		253
2	3rd order	413
3		613

low-speed maneuvering MMG model and captive model tests. Hereafter, the model for comparison will be referred to as thereference model.

Details of the model and parameters used in reference model are as follows: the MMG model estimates the hydrodynamic forces generated by each module, such as the hull, propeller, rudder, and wind force. The sub-modules used in reference model are as follows: Yoshimura's model [56] for the hull; Fujiwara's model [38] for the wind pressure; and Kang's model [57] for the propeller and rudder forces.

Table 5 Settings of computational cases with 2nd-order models

Case no.	Order	SM	α	λ
1	2nd	2	0	0
2			0	$1e2$
3			$1e2$	0
4			$1e2$	$1e2$
5	2nd	3	0	0
6			0	$1e2$
7			$1e2$	0
8			$1e2$	$1e2$
9	2nd	4	0	0
10			0	$1e2$
11			$1e2$	0
12			$1e2$	$1e2$

Model parameters were obtained by a captive model test of the subject ship, empirical formulae, or substituted by other ship's parameters. Specifically, for the hull model, the linear coefficient and the astern drag coefficient were derived from captive model tests, while the other values were obtained by

Table 6 Settings of computational cases with 3rd-order models

Case no.	Order	SM	α	λ
13	3rd	2	0	0
14			0	$1e2$
15			0	$1e4$
16			$1e2$	0
17			$1e2$	$1e2$
18			$1e2$	$1e4$
19			$1e4$	0
20			$1e4$	$1e2$
21	3rd	3	0	0
22			0	$1e2$
23			0	$1e4$
24			$1e2$	0
25			$1e2$	$1e2$
26			$1e2$	$1e4$
27			$1e4$	0
28			$1e4$	$1e2$

empirical formulae [56]. For the propeller and rudder models, propeller thrust coefficients K_{T0}, K_{T1}, K_{T2} were obtained from the propeller open test of the subject ship's propeller, and the other coefficients were substituted by VLCC's values given by Kang [57]. Wind coefficients were derived by Fujiwara's regression formulae using the subject ship's geometric parameters. Although the reference model used surrogate parameters for more than half of its parameters, the authors believe that the reference model has sufficient accuracy for practical use because the authors used the reference model to train an automatic berthing controller and successfully demonstrated a scaled-model experiment of automatic berthing [34].

4 Results

In this chapter, we examine the performance of the optimal parameter $\boldsymbol{\theta}_{\mathrm{opt}}$ obtained from the optimization. First, we select the optimal parameter for each computational case by observing the learning curve of train loss $\mathcal{L}(\boldsymbol{\theta}; \mathcal{D}^{(\mathrm{train})})$ and validation loss $\mathcal{L}(\boldsymbol{\theta}; \mathcal{D}^{(\mathrm{validation})})$. Second, since CMA-ES is a stochastic search method, we check the dependency on the random seed used in CMA-ES. Third, we select the optimal value of hyperparameters by comparing the $\mathcal{L}(\boldsymbol{\theta}_{\mathrm{opt}}; \mathcal{D}^{(\mathrm{validation})})$ with different hyperparameter values. Finally, the generalization performance is checked using random maneuvering test set $\mathcal{D}^{(\mathrm{test})}$ and crash-astern test set $\mathcal{D}^{(\mathrm{CA})}$. We also check how the performance varies with the order of model formulae and the Submodel. Furthermore, the estimation error in train, validation, and test is discussed.

The error norm $\mathcal{L}$ defined by Eq. 21 is used as a performance metric. This is because the objective function $\mathcal{F}$ shown in Eq. 20 is penalized by two terms other than the error norm.

4.1 Learning curve of optimization

The optimization yields the optimal parameter $\boldsymbol{\theta}_{\mathrm{opt}}^{(\mathrm{train})}$ in $\mathcal{D}^{(\mathrm{train})}$ defined by Eq. 19, but overfitting may occur. Thus, the error norm $\mathcal{L}^{(\mathrm{validation})} \equiv \mathcal{L}(\boldsymbol{\theta}; \mathcal{D}^{(\mathrm{validation})})$ on $\mathcal{D}^{(\mathrm{validation})}$ is shown below:

$$\mathcal{L}(\boldsymbol{\theta}; \mathcal{D}^{(\mathrm{validation})}) = \sum_{i=1}^{N} \int_{t=0}^{t_{\mathrm{f}}} \|\hat{\boldsymbol{s}}_t^{(\mathrm{validation},i)} - \hat{\boldsymbol{s}}_t^{(\mathrm{sim},i)}(\boldsymbol{\theta})\|^2 \mathrm{d}t \tag{36}$$

and $\mathcal{L}^{(\mathrm{train})}$ are observed during iterative process of optimization. Figure 4 shows the learning curve of two representative computational cases. Note that in Fig. 4, the mean of the candidate solutions $\overline{\boldsymbol{\theta}}$ of each iteration of the CMA-ES was used for error norm $\mathcal{L}^{(\mathrm{train})}$, $\mathcal{L}^{(\mathrm{validation})}$ by Eqs. 21, 36. Since the total time of datasets is different, the error norms were compared in error-per-time from $(\mathcal{L}/T)$ using the data set time $T^{(\mathrm{train})}$, $T^{(\mathrm{validation})}$. Note that $\mathcal{L}^{(\mathrm{train})}$ and $\mathcal{L}^{(\mathrm{validation})}$ have several peaks at the same iterations in Fig. 4. This is due to the restart strategy of CMA-ES.

The learning curve of the SM-2, 3rd-order model is shown in Fig. 4a. The validation loss $\mathcal{L}^{(\mathrm{validation})}$, indicated by the blue line, showed the same downward trend as training loss $\mathcal{L}^{(\mathrm{train})}$. The validation loss stagnated at the value with slight degradation from its minimum indicated by the blue circle. Therefore, we concluded that overfitting did not occur in this computational case. On the other hand, in the SM-3, 3rd-order model, shown in Fig. 4b, $\mathcal{L}^{(\mathrm{validation})}$ worsened in the iteration around $\bar{\boldsymbol{\theta}}_{\mathrm{opt}}^{(\mathrm{train})}$ indicated by the black circle; thus, we concluded that overfitting has occurred.

To avoid overfitting, the optimal parameter on $\mathcal{D}^{(\mathrm{validation})}$ was selected as the optimal parameter for each computational case, and the model with the optimal parameter $\boldsymbol{\theta}_{\mathrm{opt}}^{(\mathrm{validation})}$ was defined as the optimal model. More precisely, the optimal parameter $\boldsymbol{\theta}_{\mathrm{opt}}^{(\mathrm{validation})}$ was selected from the set $\Theta^{(\mathrm{train})}$, which is the set of $\overline{\boldsymbol{\theta}}$ per 200 iterations:

$$\boldsymbol{\theta}_{\mathrm{opt}}^{(\mathrm{validation})} = \underset{\overline{\boldsymbol{\theta}} \in \Theta^{(\mathrm{train})}}{\mathrm{argmin}}\, \mathcal{L}(\overline{\boldsymbol{\theta}}; \mathcal{D}^{(\mathrm{validation})}). \tag{37}$$

4.2 Random seed trial

Since CMA-ES is a stochastic search method, the optimal parameter may depend on the random seed. Before testing

the performance of the optimal model, we check the effect of the random seed. Here, we performed five independent trials with different random number seeds for representative cases. Random seed trials with regularization penalty λ and deviation penalty α were only conducted for 3rd-order models. Trials on the cases with $\alpha = 0$ or $\lambda = 0$ were conducted both on 2nd-order and 3rd-order models. From now on, for simplicity of notation, the error norm is expressed in the following expression:

$$\begin{aligned} \mathcal{L}'^{(\mathrm{train})}_{\mathrm{opt}} &= \mathcal{L}(\boldsymbol{\theta}^{(\mathrm{train})}_{\mathrm{opt}};\mathcal{D}^{(\mathrm{train})})/T^{(\mathrm{train})} \\ \mathcal{L}'^{(\mathrm{validation})}_{\mathrm{opt}} &= \mathcal{L}(\boldsymbol{\theta}^{(\mathrm{validation})}_{\mathrm{opt}};\mathcal{D}^{(\mathrm{validation})})/T^{(\mathrm{validation})}. \end{aligned} \tag{38}$$

The effect of random seed on the error norm $\mathcal{L}$ is shown in Fig. 5. In all cases except for the SM-3, 3rd-order model, $\alpha = 0,\ \lambda = 1e2$ shown in yellow, the error norm is smaller than that of the reference model for both training and validation dataset regardless of the random seed, indicating that the model obtained by the proposed method has the same or better estimation performance than the existing methods.

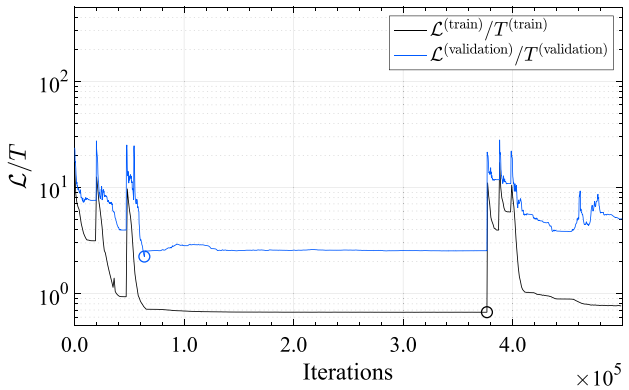

(a) SM-2, 3rd order model, $\alpha = 0,\ \lambda = 0$.

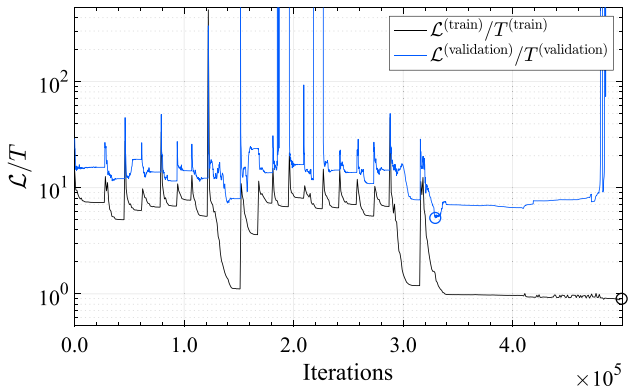

(b) SM-3, 3rd order model, $\alpha = 0,\ \lambda = 0$.

Fig. 4 Train loss and validation loss through the optimization by CMA-ES. Black circle represents $\mathcal{L}(\boldsymbol{\theta}^{(\mathrm{train})}_{\mathrm{opt}};\mathcal{D}^{(\mathrm{train})})$ and blue circle represents $\mathcal{L}(\boldsymbol{\theta}^{(\mathrm{validation})}_{\mathrm{opt}};\mathcal{D}^{(\mathrm{validation})})$. Note that in Fig. 4, line plots of $\mathcal{L}^{(\mathrm{validation})}/T^{(\mathrm{validation})}$ are not connected when the error norm is much greater than max of vertical axis range: $\mathcal{L}^{(\mathrm{validation})}/T^{(\mathrm{validation})} \gg 5 \times 10^2$. Other peaks in the figure are due to the restart strategy of CMA-ES. "SM" stands for Submodel

Next, we discuss the differences in performance for each computational case on the training and validation datasets. First, we focus on $\mathcal{L}'^{(\mathrm{train})}_{\mathrm{opt}}$. In $\mathcal{L}'^{(\mathrm{train})}_{\mathrm{opt}}$, the third-order model has a smaller error norm $\mathcal{L}'^{(\mathrm{train})}_{\mathrm{opt}}$ than the second-order model, which means that it fits the training data better. The effect of the regularization penalty λ and the deviation penalty α differed depending on the model. In the SM-2, 3rd-order model, $\alpha,\ \lambda$ tended to suppress the variation of $\mathcal{L}'^{(\mathrm{train})}_{\mathrm{opt}}$. On the other hand, in the SM-3, 3rd-order model, the variation of $\mathcal{L}'^{(\mathrm{train})}_{\mathrm{opt}}$ was larger. Moreover, on $\lambda = 1e2$ case, $\mathcal{L}'^{(\mathrm{train})}_{\mathrm{opt}}$ was significantly worsen. Therefore, the effect of α and λ on optimization is different for each model. A parameter study of the hyperparameters is required for each model when using the proposed method.

Next, we focus on $\mathcal{L}'^{(\mathrm{validation})}_{\mathrm{opt}}$. Although $\mathcal{L}'^{(\mathrm{validation})}_{\mathrm{opt}}$ is several times worse than that of $\mathcal{L}'^{(\mathrm{train})}_{\mathrm{opt}}$, $\mathcal{L}^{(\mathrm{validation})}_{\mathrm{opt}}$ is still smaller than that of the reference model except for one case. In other words, the proposed method has the same or better estimation accuracy than the conventional method even when the data is not used for training, as long as the appropriate α and λ were selected, regardless of the random seed.

The performance rank of the models on $\mathcal{D}^{(\mathrm{validation})}$ is the same as for training: SM-2, 3rd-order model is the best, followed by SM-3, 3rd-order model. The second-order model is inferior to the third-order model, and the performance difference between the second-order models is insignificant compared to the variation due to random seeding. Moreover, as in training, the trend of the regularization penalty λ and the deviation penalty α differed among the models. In the SM-2, 3rd-order model, the regularization penalty λ and the deviation penalty α suppressed the variation of $\mathcal{L}'^{(\mathrm{validation})}_{\mathrm{opt}}$. In SM-3, 3rd-order model, $\alpha = 0,\ \lambda = 1e2$ is an exception where $\mathcal{L}'^{(\mathrm{validation})}_{\mathrm{opt}}$ is worse than the other cases. This may be because proper learning is not achieved as described in the previous paragraph, resulting in worse performance for $\mathcal{L}'^{(\mathrm{validation})}_{\mathrm{opt}}$.

4.3 Select the best hyperparameter

In the previous section, we discussed the effect of random seeding on performance estimation. We found that α and λ show different trends depending on the model. Therefore, we next select the hyperparameters: α and λ, based on the performance on $\mathcal{D}^{(\mathrm{validation})}$. The error norm $\mathcal{L}'^{(\mathrm{train})}_{\mathrm{opt}}$ and $\mathcal{L}'^{(\mathrm{validation})}_{\mathrm{opt}}$ of the optimal model for all computational

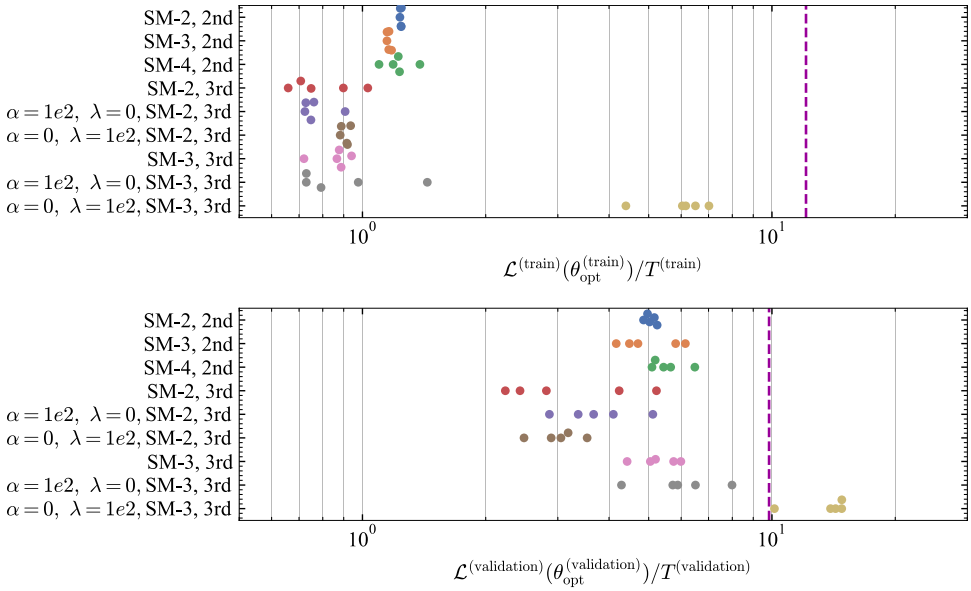

Fig. 5 Results of random seed trial. Dot plots represent each random seed trial. Labels on vertical axis without α and λ values, those are $\alpha = 0,\ \lambda = 0$. The vertical purple dashed line represents reference model results

cases defined in Tables 5, 6 is shown in Fig. 6. In Fig. 6a, dot plots of $\mathcal{L}'^{(\mathrm{train})}_{\mathrm{opt}}$, $\mathcal{L}'^{(\mathrm{validation})}_{\mathrm{opt}}$ are color-coded by α values, and in Fig. 6b, dot plots are color-coded by λ values.

For $\mathcal{D}^{(\mathrm{train})}$, the fitness was higher when the value of α and λ was close to zero. For $\mathcal{D}^{(\mathrm{validation})}$, the same trend was seen for λ, but there was no clear trend due to the deviation penalty α. Since the deviation penalty and regularization are intended to prevent overestimation of acceleration and overfitting, both caused by the complexity of the proposed model, the appropriate value is expected to depend on the characteristics of the model and dataset. However, we could not observe any clear performance degradation due to the penalties. Therefore, when using the proposed method, the user is recommended to perform parameter studies on the validation dataset for α and λ. For example, we introduced penalties to expect a regularization effect for models with high searching dimensions, but $\lambda = 1e4$ has worse $\mathcal{L}'^{(\mathrm{train})}_{\mathrm{opt}}$, $\mathcal{L}'^{(\mathrm{validation})}_{\mathrm{opt}}$ are both worse than in the other cases, suggesting that the regularization penalty was too large.

In the next section, we selected the combination of $\alpha,\ \lambda$ that minimize $\mathcal{L}^{(\mathrm{validation})}$ for each model, and compared the performance of each model with the test data.

4.4 Evaluation by test data

The generalization performance of the optimal models is checked on the test data. As with training and validation, the following simplified notations are made for test and crash-astern:

$$\begin{aligned}\mathcal{L}'^{(\mathrm{test})}_{\mathrm{opt}} &= \mathcal{L}(\boldsymbol{\theta}^{(\mathrm{validation})}_{\mathrm{opt}};\mathcal{D}^{(\mathrm{test})})/T^{(\mathrm{test})}\\ \mathcal{L}'^{(\mathrm{CA})}_{\mathrm{opt}} &= \mathcal{L}(\boldsymbol{\theta}^{(\mathrm{validation})}_{\mathrm{opt}};\mathcal{D}^{(\mathrm{CA})})/T^{(\mathrm{CA})}\end{aligned} \tag{39}$$

4.4.1 Random maneuvers

The test data results for the optimal model for each model are shown in Fig. 7a. The figure shows that all the optimal models outperform the reference in $\mathcal{D}^{(\mathrm{test})}$. The plots are generally on the linear line shown by the dashed line in the figure. In other words, the optimal parameter $\boldsymbol{\theta}^{(\mathrm{validation})}_{\mathrm{opt}}$ chosen by the $\mathcal{D}^{(\mathrm{validation})}$ achieves the same accuracy with unknown test data. The reference model is also on the same line, indicating that the proposed method has a generalization performance that can maintain its estimation accuracy regardless of the data set under random maneuvers, which is the same as reference model.

Next, we show the results of the maneuvering simulation using the best optimal model and the worst optimal model to verify the performance of the proposed model in detail. Based on the Fig. 7a, SM-2, 2nd-order model, $\alpha = 0,\ \lambda = 0$, is the worst, and the SM-2, 3rd-order model, $\alpha = 0,\ \lambda = 0$ is the best. The maneuvering simulation results of the two models are shown in Fig. 8. The simulation results of the reference model and the time series of $\mathcal{D}^{(\mathrm{test})}$ are also compared. The simulation results from both optimal models agreed with the experimental results. In addition, the acceleration $\dot{\boldsymbol{s}}_t = (\dot{u},\ \dot{v}_{\mathrm{m}},\ \dot{r})$ of the optimal model and the reference model are of the same order. In other words, the proposed model with optimal parameters can obtain the same level of acceleration as the reference model, which is a model constructed

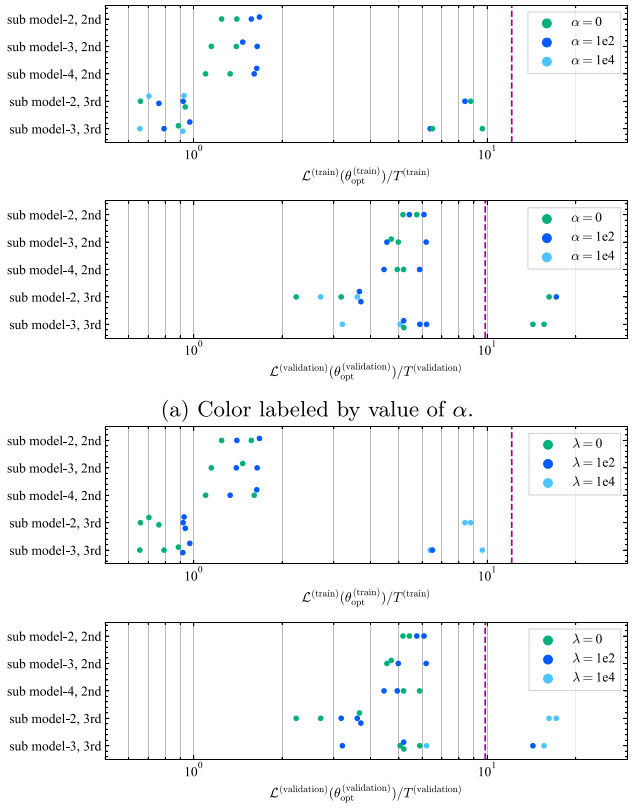

(a) Color labeled by value of α.

(b) Color labeled by value of λ.

Fig. 6 Relation between hyperparameters and estimation performance of the optimal model. The vertical purple dashed line represents reference model results

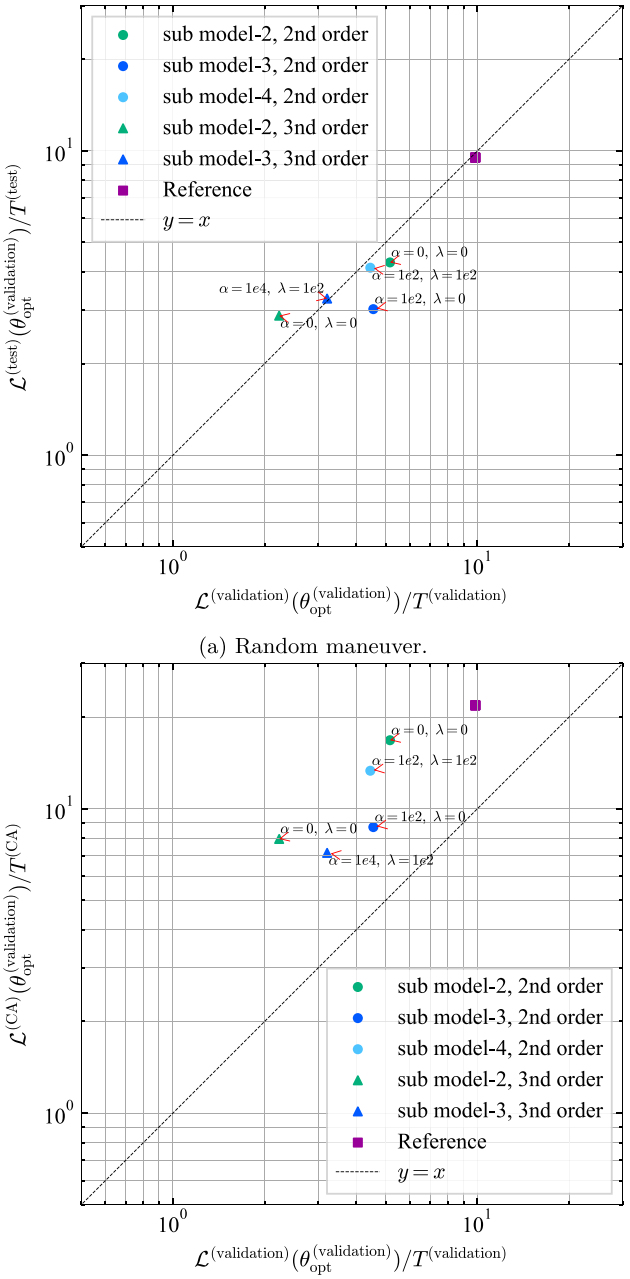

(a) Random maneuver.

(b) Crash-astern.

Fig. 7 Performance on test dataset $\mathcal{D}^{(\mathrm{test})}$ and $\mathcal{D}^{(\mathrm{CA})}$

from hydrodynamic forces measured by model tests even though the acceleration is not included in the optimization of the proposed model.

4.4.2 Crash-astern

Here we validate the proposed model for maneuvers other than random maneuvers using the crash-astern (CA) test data set $\mathcal{D}^{(\mathrm{CA})}$. The error norm for each model is shown in Fig. 7b. The correlation coefficient between $\mathcal{L}'^{(\mathrm{validation})}_{\mathrm{opt}}$ and $\mathcal{L}'^{(\mathrm{CA})}_{\mathrm{opt}}$ is $r = 0.76$ and positively correlated. In other words, by improving the performance on random maneuvers, performance could be improved even for data with different types of maneuvers. As shown in Fig. 3, the distributions of $\mathcal{D}^{(\mathrm{train})}$ and $\mathcal{D}^{(\mathrm{CA})}$ are different. Consequently, the proposed method can improve the estimation performance for various motions and generate a stable model. Compared to $\mathcal{D}^{(\mathrm{test})}$, $\mathcal{L}$ increased by a factor of 2 to 3, which means the estimation accuracy worsened, but the reference model also showed a similar degree of deterioration.

The time series of the maneuvering simulation with the best model are compared with the physical experiment results. The results of maneuvering simulation using the best and worst model for $\mathcal{D}^{(\mathrm{CA})}$ are shown in Figs. 9 and 10. In Figs. 9 and 10, one of the four CA tests included in $\mathcal{D}^{(\mathrm{CA})}$ is shown. This particular CA test has the smallest $\mathcal{L}'^{(\mathrm{CA})}_{\mathrm{opt}}$ with simulation using the best model. The trajectory $(x_0,\ y_0,\ \psi)$ shown in Fig. 9 agrees with the experimental trajectory well except for ψ immediately after the start of the stopping

maneuver in both optimal models and during astern in the worst model. In addition, the time series of $\boldsymbol{s}_t^{(\mathrm{sim})}$ and $\dot{\boldsymbol{s}}_t^{(\mathrm{sim})}$ is shown in Fig. 10. In both the best and the worst model's results, the estimation performance of time-series showed two types of trend on contiguous subsequences (CS): CS with a good agreement and CS with a large discrepancy. In particular, the deviations were considerable for the CS at $100 < t < 200$ s immediately after the start of the crash-astern steering. Moreover, slopes of v_{m}, r had opposite signs with the experiment at $100 < t < 120$ s. The velocity slope, i.e., acceleration, is not resolved correctly, meaning transient characteristics of hydrodynamic forces are not represented at that period. In this period, $u = 0.5$ m/s at $t = 0$ of the subsequence, which is the velocity extrapolated from the training data as shown in Fig. 3. The extrapolation of the training data is considered to have degraded the estimation performance.

4.4.3 Analysis on error

This section analyzes the distribution of errors in the maneuvering simulations for each data set, to summarize the estimation performance on the training, validation, and test-CA datasets. The model used is the best model, SM-2, 3rd-order model, $\alpha = \lambda = 0$. Since the error function Eqs. 21 and 36 is the sum of errors, the squared error vector $\boldsymbol{\varepsilon}_t \equiv \left(\varepsilon_{t,u},\ \varepsilon_{t,v_{\mathrm{m}}},\ \varepsilon_{t,r}\right) \in \mathbb{R}^3$ at time t is analyzed. Here, the following equation defines the j-th component of $\boldsymbol{\varepsilon}_t$ as follows:

$$\varepsilon_{t,j} = \left\{\hat{s}_{t,j}^{(\mathrm{input},i)} - \hat{s}_{t,j}^{(\mathrm{sim},i)}(\boldsymbol{\theta}_{\mathrm{opt}};\ \mathcal{D}^{(\mathrm{input})})\right\}^2. \tag{40}$$

Here, $\hat{s}_{t,j}^{(\cdot,i)}$ is the j-th component of the standardized state variables at time t of the ith CS. The standardized state variables are $\hat{\boldsymbol{s}}_t^{(\cdot,i)} = \left(\hat{u}^{(\cdot,i)}(t),\ \hat{v}_{\mathrm{m}}^{(\cdot,i)}(t),\ \hat{r}^{(\cdot,i)}(t)\right)$.

The histogram of $\boldsymbol{\varepsilon}_t$ is shown in Fig. 11a and the cumulative frequency histogram of $\boldsymbol{\varepsilon}_t$ is shown in Fig. 11b. The figure shows that test-CA contains larger instantaneous errors than training and validation. In test-CA, v_{m} and r have longer legs of the distribution than u, which means v_{m} and r contain larger instantaneous errors. In addition, cumulative frequencies of $\varepsilon_{t,v_{\mathrm{m}}}$, $\varepsilon_{t,r}$ increased gradually for $\varepsilon_{t,j} > 15$. From this result, we can say that a specific large instantaneous error does not increase the sum of errors; instantaneous errors of about 5–10% of the overall time steps are worsening. Therefore, measures to improve the accuracy of these lower 5–10% time steps of v_{m} and r are needed.

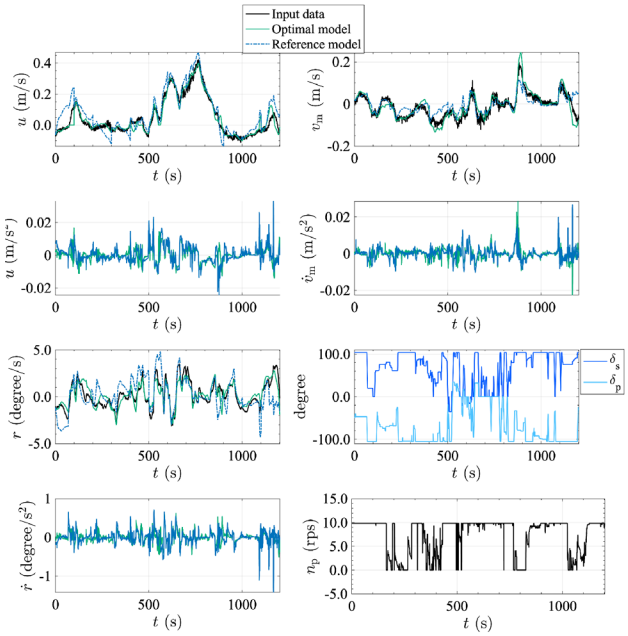

(a) Best model; SM-2, 3rd order model, $\alpha = 0,\ \lambda = 0$.

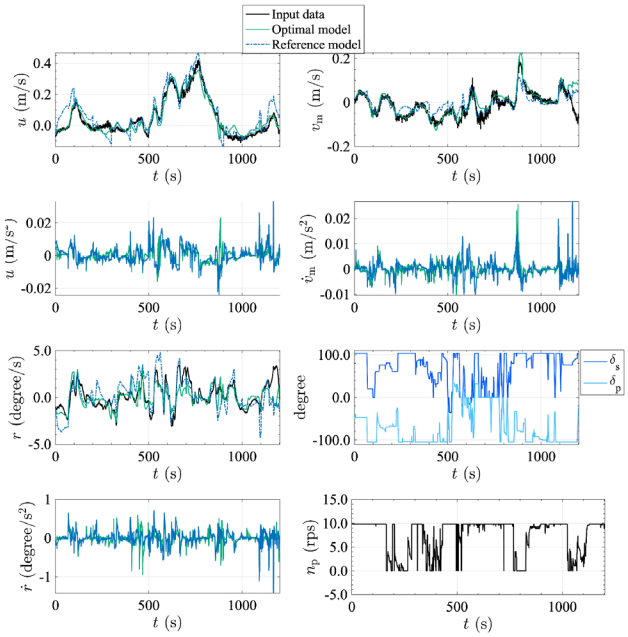

(b) Worst model; SM-2, 2nd order model; $\alpha = 0,\ \lambda = 0$.

Fig. 8 Result of maneuvering simulation on $\mathcal{D}^{(\mathrm{test})}$ by optimal models of the best model and worst model. This figure shows time histories of $\boldsymbol{s}_t^{(\mathrm{sim})}$ and $\dot{\boldsymbol{s}}_t^{(\mathrm{sim})}$ of maneuvering simulation using the optimal model and the reference model for $\mathcal{D}^{(\mathrm{test})}$. This figure also shows time histories of $\boldsymbol{a}_t$ and the measured state of the free-running model test $\boldsymbol{s}_t^{(\mathrm{test})}$

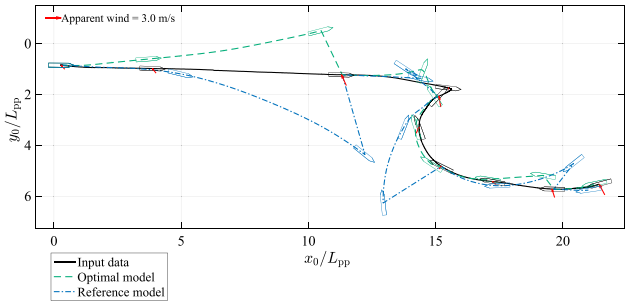

(a) Best model; SM-2, 3rd order model; $\alpha = 0,\ \lambda = 0$.

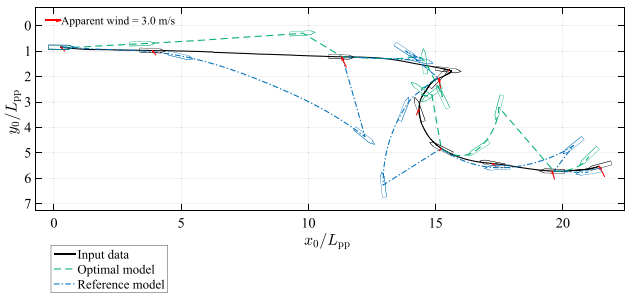

(b) Worst model; SM-2, 2nd order model; $\alpha = 0,\ \lambda = 0$.

Fig. 9 Estimated trajectories of maneuvering simulation using two optimal models and the reference model for $\mathcal{D}^{(\mathrm{CA})}$. Ship-like pentagons represent ship positions and headings at contiguous subsequences (CS)'s beginning, middle, and end. The black line represents the input dataset, i.e., measured trajectory of the free-running model test. Optimal model is SM-2, 2nd-order, $\alpha = 0,\ \lambda = 0$. Note that estimated trajectories seem to jump when the CS changes

5 Discussion

5.1 Modeling automation

Before concluding the study, we explain how the proposed model and method enable modeling automation. First, because of the simple rules for of the model formulae, derivation can be automated. Several model formulae with different terms and order numbers can easily derived for comparison. In contrast, existing hydrodynamic models must derive the expression based on hydrodynamics for each actuator configuration. Second, the necessary inputs for the proposed method are only the dataset. Generation of datasets itself cannot be automated with the proposed method; however, a priori hydrodynamic information other than the dataset is not necessary. Since CMA-ES with the restart strategy is a quasi-parameter-free optimization [55], the user is not required to seek the parameter for the optimization itself. Third, selection of the model formulae can also be automated. This can be achieved by the combination of the automated derivation of multiple model formulae with different terms or order numbers andthe determination of best model formula based on the comparison of a single fitness function, $\mathcal{L}'^{(\mathrm{validation})}_{\mathrm{opt}}$. Because of those three reasons, the proposed method can essentially remove the human work required to generatemathematical models. By employing the proposed method, we can develop an algorithm that automatically generates a model suitable for harbor maneuvers once the user feeds a dataset.

5.2 Limitations and future work

The main drawback of the proposed method is the computation time required for optimization. The SM-2, 2nd-order model, a model with the smallest number of parameters, requires three days of computation time, and the SM-3, 3rd-order model, the largest number of parameters, requires ten days. The computation conditions were 16 parallel Intel Xeon Platinum 8260 computers, and the language and compiler were Fortran 90 and Intel Fortran. CMA-ES is easy to parallelize and may be faster depending on machine power, but it is computationally expensive in general because of the need for parallel-capable machines.

A remaining issue is a dependence on the dataset size. In this study, the dataset size was kept constant. A total of approximately 10,000 s of random maneuvers were used. If $L_{\mathrm{pp}} = 100$m, this corresponds to about 16 h. As the size of the target vessel increases, the cost of data acquisition also increases. Therefore, in addition to the dependence on the amount of data, reducing the amount of data required and efficient methods of data acquisition is also future work. In addition, introducing non-dimensionalization without velocity U, such as [58], may ease the domain boundary setting of coefficients.

Another remaining issue consists of the derivation rules of mathematical expression of model formulae. As shown in Sect. 2.2.2, we modified or removed several terms in the polynomial derived by the Taylor expansion. Those modifications might affect the performance of the model.For instance, we have ignored the terms which include $\sin^2\delta$. However, those terms have non-negligible meanings on the MMG model's rudder force drag componentX_R when the ship is moving straight forward:

$$\begin{aligned} X_R &= -(1-t_R)0.5\rho A_R U_R^2 f_\alpha \sin\alpha_R \sin\delta \\ &\approx -(1-t_R)0.5\rho A_R U_R^2 f_\alpha \sin\delta\sin\delta \qquad \text{if } \alpha_R \approx \delta. \end{aligned} \tag{41}$$

Hence, further research on the derivation rule might be necessary.

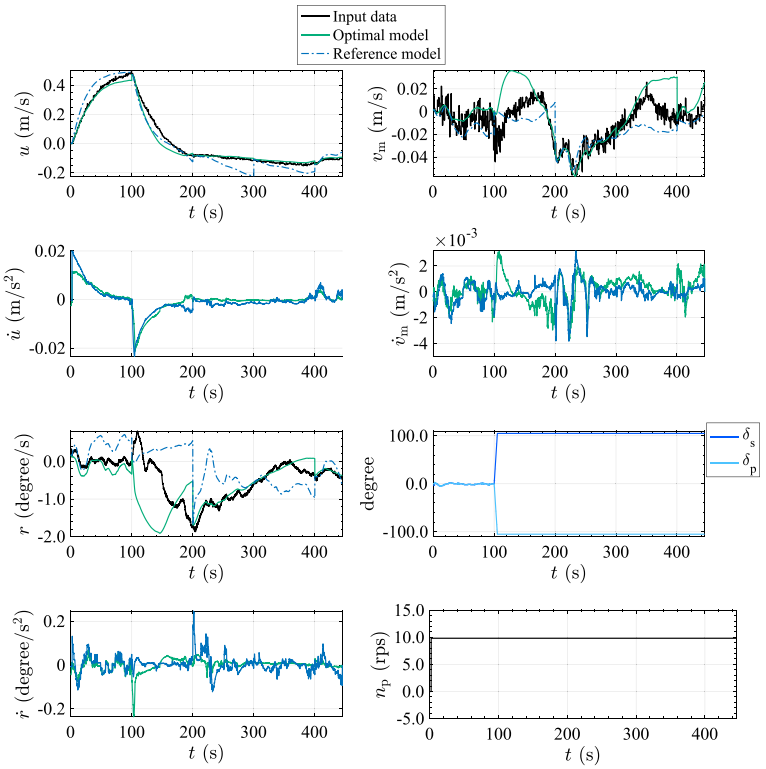

(a) Best model; SM-2, 3rd order model; $\alpha = 0,\ \lambda = 0$.

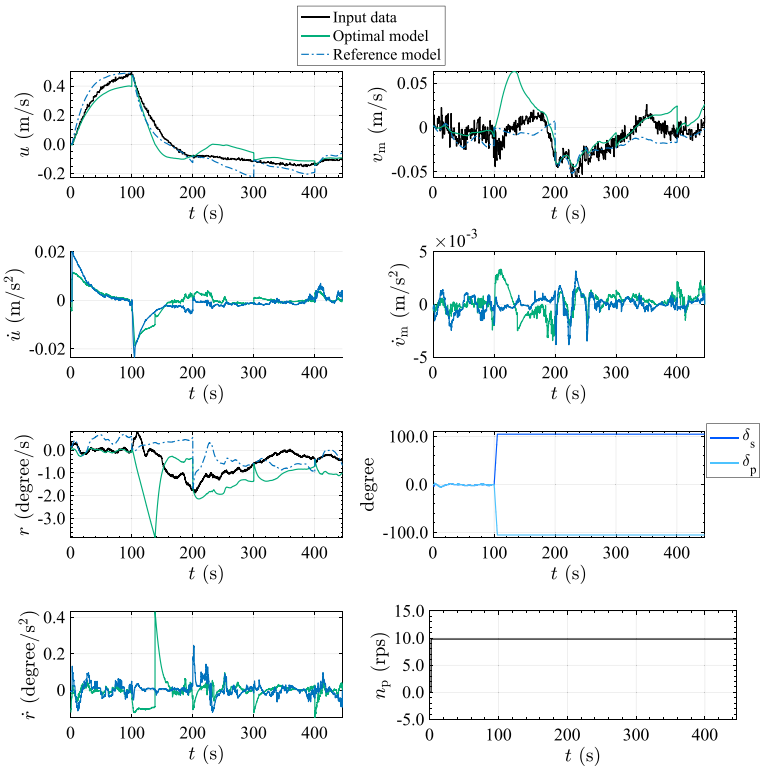

(b) Worst model; SM-2, 2nd order model; $\alpha = 0,\ \lambda = 0$.

Fig. 10 Time histories of $\boldsymbol{s}_t^{(\mathrm{sim})}$ and $\dot{\boldsymbol{s}}_t^{(\mathrm{sim})}$ of maneuvering simulation using the best optimal model and the reference model for $\mathcal{D}^{(\mathrm{CA})}$. This figure also shows time histories of control inputs and $\boldsymbol{s}_t^{(\mathrm{CA})}$, i.e., measured state of free-running model test. Optimal model is SM-2, 2nd order, $\alpha = 0,\ \lambda = 0$

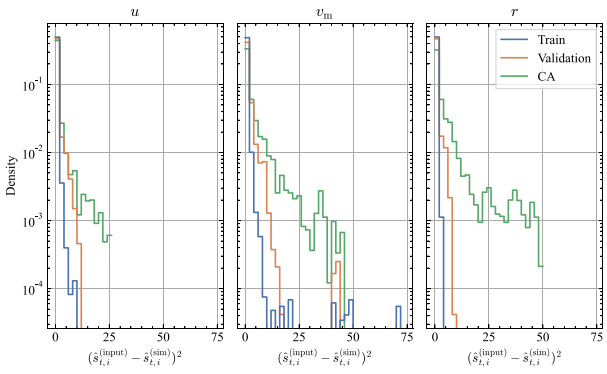

(a) Histogram of instantaneous errors in log scale vertical axis.

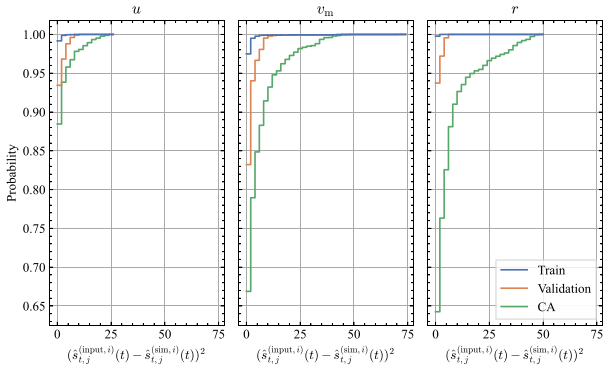

(b) Cumulative histogram of errors.

Fig. 11 Histograms of instantaneous error $\boldsymbol{\varepsilon}_t = \left(\varepsilon_{t,u}, \varepsilon_{t,v_m}, \varepsilon_{t,r}\right)$ per data sets: $\mathcal{D}^{(\mathrm{train})}$, $\mathcal{D}^{(\mathrm{validation})}$ and $\mathcal{D}^{(\mathrm{CA})}$

6 Conclusion

In this study, we proposed the Abkowitz–MMG hybridmodel and its parameter identification method for harbor maneuvers and to realize automated modeling.

The proposed model can be derived according to simple rules using Taylor expansion and has a high degree of freedom to express harbor maneuvers' complex motions and ship handlings. The proposed model can be more easily derived than existing Hydrodynamic models for arbitrary ship configurations. In addition, the physical meaning of the model's formulae and their terms is much more understandable than those using neural networks.

We also proposed a method to identify the model parameters and select the model's formulae using system identification. Even though the proposed model needs to identify several hundred model parameters because of its simple rules for derivation, SI using CMA-ES enables identifying model parameters within reasonable computational time. Moreover, since multiple models can be easily derived, we identified the parameters of several models and selected the best model from them. Thus, the proposed method does not depend on the captive model tests and knowledge of ship hydrodynamics to select appropriate mathematical expressions of the model, thereby reducing the amount of labor required for model selection. In addition, simple rule-based model derivation and easy model selection methods can relax the necessary skill and facility requirements for users to perform model generation.

This study used trajectories of a free-running model ship of a single-propeller, VecTwin-rudder-equipped ship, as the data set. As a result, we confirmed that even a mathematical model derived from simple rules could estimate unknown harbor maneuvers equivalently or more accurately than a model generated by existing methods.

In summary, we showed that the proposed model and method could reduce human intervention in model generation and have adequate estimation performance. Consequently, they enable automated modeling, which automates the modeling process itself. Although design and development of the automation algorithm are the remaining tasks, the basic concept of modeling automation, and the core of the automation algorithm, i.e., the mathematical model and the model generation method, were proposed in this study.

Acknowledgements This study was conducted as a part of the Nippon Foundation's "demonstration tests of The Nippon Foundation MEGURI2040 Fully Autonomous Ship Program." This study was also supported by a Grant-in-Aid for Scientific Research from the Japan Society for Promotion of Science (JSPS KAKENHI Grant #22H01701). This study was conducted under a joint research project between Japan Hamworthy Co., Ltd. and Osaka University. The authors would like to express gratitude to Prof. Masaaki Sano at Hiroshima University, for providing captive model test results. The authors would like to thank Prof. Naoya Umeda at Osaka University for insightful advise during this research. The authors also would like to thank students of the Ship Intelligentization Subarea, Osaka University, for supporting the model experiment: Dimas M. Rachman, Nozomi Amano, Hiroaki Koike, and Yuta Fueki.

Funding Open Access funding provided by Osaka University.

Data availability Due to the nature of the research, participants of this study did not agree for their data to be shared publicly, so supporting data is not available.

References

1. Miyauchi Y, Maki A, Umeda N, Rachman DM, Akimoto Y (2022) System parameter exploration of ship maneuvering model for automatic docking/berthing using CMA-ES. J Mar Sci Technol 27:1065
2. Yasukawa H, Ishikawa T, Yoshimura Y (2021) Investigation on the rudder force of a ship in large drifting conditions with the mmg model. J Mar Sci Technol 26:1078
3. Abkowitz MA (1980) Measurement of hydrodynamic characteristics from ship maneuvering trials by system identification. Trans Soc Nav Archit Mar Eng 88:283–318
4. Fossen TI (2021) Handbook of marine craft hydrodynamics and motion control, 2nd edn. Wiley, New York
5. Manoeuvring Committee of the 29th ITTC (2021) ITTC—Recommended Procedures and Guidelines, Captive Model Test
6. Chislett MS, Strom-Tejsen J (1965) Planar motion mechanism tests and full-scale steering and manoeuvring predictions for a mariner class vessel. Int Shipbuild Prog 12:201
7. Yasukawa H, Yoshimura Y (2015) Introduction of MMG standard method for ship maneuvering predictions. J Mar Sci Technol (Japan) 20(1):37
8. Shouji K, Ohtsu K, Mizoguchi S (1992) An automatic berthing study by optimal control techniques. IFAC Proc Vol 25:185
9. Hasegawa K, Fukutomi T (1994) On harbour manoeuvring and neural control system for berthing with tug operation. In: Proc. of 3rd International conference manoeuvring and control of marine craft (MCMC'94), pp 197–210
10. Maki A, Sakamoto N, Akimoto Y, Nishikawa H, Umeda N (2020) Application of optimal control theory based on the evolution strategy (CMA-ES) to automatic berthing. J Mar Sci Technol (Japan) 25(1):221
11. Maki A, Akimoto Y, Naoya U (2021) Application of optimal control theory based on the evolution strategy (cma-es) to automatic berthing (part: 2). J Mar Sci Technol 26:835
12. Miyauchi Y, Sawada R, Akimoto Y, Umeda N, Maki A (2022) Optimization on planning of trajectory and control of autonomous berthing and unberthing for the realistic port geometry. Ocean Eng 245:110390
13. Rachman DM, Maki A, Miyauchi Y, Umeda N (2022) Warm-started semionline trajectory planner for ship's automatic docking (berthing). Ocean Eng 252:111127
14. Shimizu S, Nishihara K, Miyauchi Y, Wakita K, Suyama R, Maki A, Shirakawa S (2022) Automatic berthing using supervised learning and reinforcement learning. Ocean Eng 265:112553
15. Akimoto Y, Miyauchi Y, Maki A (2022) Saddle point optimization with approximate minimization oracle and its application to robust berthing control. ACM Trans Evol Learn Optim 2:1
16. Stern F, Agdraup K, Kim SY, Hochbaum AC, Rhee KP, Quadvlieg F, Perdon P, Hino T, Broglia R, Gorski J (2011) Experience from SIMMAN 2008—the first workshop on verification and validation of ship maneuvering simulation methods. J Ship Res 55(02):135
17. Peng Guo H, Jian Zou Z, Peng Guo H, Jian Zou Z (2017) System-based investigation on 4-DOF ship maneuvering with hydrodynamic derivatives determined by RANS simulation of captive model tests. Appl Ocean Res 68:11
18. Sakamoto N, Ohashi K, Araki M, ichi Kume K, Kobayashi H (2019) Identification of kvlcc2 manoeuvring parameters for a modular-type mathematical model by rans method with an overset approach. Ocean Eng 188:106257
19. Åström KJ, Källström CG (1976) Identification of ship steering dynamics. Automatica 12:9
20. Mei B, Sun L, Shi G (2019) White-black-box hybrid model identification based on RM-RF for ship maneuvering. IEEE Access 7:57691
21. Zhu M, Sun W, Hahn A, Wen Y, Xiao C, Tao W (2020) Adaptive modeling of maritime autonomous surface ships with uncertainty using a weighted LS-SVR robust to outliers. Ocean Eng 200:107053
22. Araki M, Sadat-Hosseini H, Sanada Y, Tanimoto K, Umeda N, Stern F (2012) Estimating maneuvering coefficients using system identification methods with experimental, system-based, and CFD free-running trial data. Ocean Eng 51:63
23. Xie S, Chu X, Liu C, Liu J, Mou J (2020) Parameter identification of ship motion model based on multi-innovation methods. J Mar Sci Technol (Japan) 25:162
24. Bai W, Ren J, Li T (2019) Modified genetic optimization-based locally weighted learning identification modeling of ship maneuvering with full scale trial. Future Gener Comput Syst 93:1036
25. Xu H, Hinostroza MA, Wang Z, Soares CG (2020) Experimental investigation of shallow water effect on vessel steering model using system identification method. Ocean Eng 199:106940
26. Organization IM (2002) Resolution MSC.137(76), STANDARDS FOR SHIP MANOEUVRABILITY. MSC 76/23/Add.1
27. Sawada R, Hirata K, Kitagawa Y, Saito E, Ueno M, Tanizawa K, Fukuto J (2020) Path following algorithm application to automatic berthing control. J Mar Sci Technol (Japan) 26:541–5
28. Pedersen AA (2019) Optimization based system identification for the milliampere ferry. Master thesis, NTNU. http://hdl.handle.net/11250/2625699
29. Ogawa A, Kasai H (1978) On the mathematical model of manoeuvring motion of ships. Int Shipbuild Prog 25(292):306
30. Nomoto K, Taguchi T, Honda K, Hirano S (1957) On the steering qualities of ships. Int Shipbuild Prog 4(35):354
31. Guedes Moreira L, Soares C (2003) Dynamic model of manoeuvrability using recursive neural networks. Ocean Eng 30(13):1669
32. Rajesh G, Bhattacharyya SK (2008) System identification for nonlinear maneuvering of large tankers using artificial neural network. Appl Ocean Res 30:256
33. Oskin DA, Dyda AA, Markin VE (2013) Neural network identification of marine ship dynamics. IFAC Proc Vol 46(33):191
34. Wakita K, Akimoto Y, Rachman DM, Miyauchi Y, Umeda N, Maki A (2022) Collision-probability reduction method of tracking control for automatic docking/berthing using reinforcement learning. J Mar Sci Technol 28(4):844–61
35. Miyauchi Y, Maki A, Akimoto Y, Umeda N (2021) 4-Quadrant Abkotwitz model applicable for complex low-speed maneuver include berthing and unberthing. In: Conference proceedings, the Japan society of naval architects and ocean engineers, vol 33, pp 49–58
36. Miyauchi Y, Akimoto Y, Umeda N, Maki A (2022) Mathematical model for VecTwin rudder system on harbor maneuver to realize modeling automation. In: Conference proceedings, the Japan society of naval architects and ocean engineers, vol 35 , pp 53–66 **(in Japanese)**
37. Abkowitz MA (1964) Lectures on ship hydrodynamics-Steering and manoeuvrability. Tech. rep., Hydro and Aerodynamic Laboratory, Lyngby
38. Fujiwara T, Ueno M, Nimura T (1998) Estimation of wind forces and moments acting on ships. J Soc Nav Archit Japan 1998(183):77
39. Matsumoto N, Suemitsu K (1980) The prediction of manoeuvring performances by captive model tests. J Kansai Soc Nav Archit Japan 176:11
40. Kose K (1982) On a new mathematical model of maneuvering motions of a ship and its applications. Int Shipbuild Prog 29:205

41. Smitt LW, Chislett MS (1972) Course stability while stopping. J Mech Eng Sci 14:181
42. Fujino M, Kirita A (1978) On the manoeuvrability of ships while stopping by adverse rotation of propeller: 1st report. J Kansai Soc Nav Archit Japan 169:57
43. Yoshimura Y, Nomoto K (1978) Modeling of manoeuvring behaviour of ships with a propeller idling, boosting and reversing. J Soc Nav Archit Japan 1978(144):57
44. Watanabe M, Sano M, Yasukawa H, Matsuda A, Hosogaya H (2022) Study on hydrodynamic force characteristics of a ship equipped with VecTwin Rudder system-modeling of the rudder normal force. In: Conference proceedings, the Japan society of naval architects and ocean engineers, vol 35, pp 335–342
45. Isherwood RM (1973) Wind resistance of merchant ships. Trans R Inst Nav Archit 115:327
46. Hamada S, Miyauchi Y, Akimoto Y, Umeda N, Maki A (2023) System identification of porpoising dynamics of high-speed planing craft using full scale trial data. Ocean Eng 270:113585
47. Hwang WY (1982) Cancellation effect and parameter identifiability of ship steering dynamics. Int Shipbuild Prog 29(332):90
48. Hansen N (2006) The CMA evolution strategy: a comparing review. Springer, Berlin, pp 75–102
49. Hansen N, Auger A, Ros R, Finck S, Pošík P (2010) Comparing results of 31 algorithms from the black-box optimization benchmarking bbob-2009. In: Proceedings of the 12th annual conference companion on genetic and evolutionary computation, New York, GECCO '10, pp 1689–1696
50. Rios LM, Sahinidis NV (2013) Derivative-free optimization: a review of algorithms and comparison of software implementations. J Glob Optim 56(3):1247
51. Akimoto Y, Hansen N (2020) Diagonal acceleration for covariance matrix adaptation evolution strategies. Evol Comput 28(3):405
52. Akimoto Y, Nagata Y, Ono I, Kobayashi S (2012) Theoretical foundation for cma-es from information geometry perspective. Algorithmica 64(4):698
53. Ollivier Y, Arnold L, Auger A, Hansen N (2017) Information-geometric optimization algorithms: a unifying picture via invariance principles. J Mach Learn Res 18(18):1
54. Sakamoto N, Akimoto Y (2017) Modified box constraint handling for the covariance matrix adaptation evolution strategy. In: Proceedings of the genetic and evolutionary computation conference companion, New York, GECCO '17, pp 183–184
55. Auger A, Hansen N (2005) A restart CMA evolution strategy with increasing population size. In: 2005 IEEE congress on evolutionary computation, vol 2. IEEE, pp. 1769–1776
56. Yoshimura Y, Nakao I, Ishibashi A (2009) Unified mathematical model for ocean and harbour manoeuvring. In: Proceedings of MARSIM2009, pp 116–124
57. Kang D, Nagarajan V, Hasegawa K, Sano M (2008) Mathematical model of single-propeller twin-rudder ship. J Mar Sci Technol 13:207
58. Kose K, Hinata H, Hashizume Y, Futagawa E (1985) 2. On a new mathematical model for manoeuvring motions of ships in low speed. Nav Archit Ocean Eng 23:15